Atmos. Chem. Phys. Discuss., doi:10.5194/acp-2015-823, 2016
Manuscript under review for journal Atmos. Chem. Phys.
Published: 19 January 2016

Atmospheric Chemistry and Physics Discussions

Aerosol optical, microphysical and radiative properties at three regional background insular sites in the western Mediterranean Basin

M. Sicard[1,2], R. Barragan[1,2], F. Dulac[3], L. Alados-Arboledas[4,5], and M. Mallet[6]

[1]Remote Sensing Laboratory, Universitat Politècnica de Catalunya, Barcelona, Spain
[2]Ciències i Tecnologies de l'Espai – Centre de Recerca de l'Aeronàutica i de l'Espai/Institut d'Estudis Espacials de Catalunya (CTE-CRAE/IEEC), Universitat Politècnica de Catalunya, Barcelona, Spain
[3]Laboratoire des Sciences du Climat et de l'Environement, IPSL/LSCE, CEA-CNRS-UVSQ, Gif-sur-Yvette, France
[4]Dpt. Applied Physics, Faculty of Sciences, University of Granada, Granada, Spain
[5]Andalusian Institute for Earth System Research (IISTA-CEAMA), Granada, Spain
[6]Laboratoire d'Aérologie, Université de Toulouse/CNRS, Toulouse, France

Received: 13 October 2015 – Accepted: 8 December 2015 – Published: 19 January 2016

Correspondence to: M. Sicard (msicard@tsc.upc.edu)

Published by Copernicus Publications on behalf of the European Geosciences Union.

ACPD

doi:10.5194/acp-2015-823

Abstract

In the framework of the ChArMEx (the Chemistry-Aerosol Mediterranean Experiment, http://charmex.lsce.ipsl.fr/) program, the seasonal variability of the aerosol optical, microphysical and radiative properties is examined in two regional background insular sites in the western Mediterranean Basin (WMB): Ersa (Corsica Island, France) and Palma de Mallorca (Mallorca Island, Spain). A third site in Alborán (Alborán Island, Spain) with only a few months of data is considered for exploring the possible Northeast–Southwest (NE–SW) gradient of the aforementioned aerosol properties. The dataset is exclusively composed of AERONET (Aerosol Robotic Network; http://aeronet.gsfc.nasa.gov/) products during a four-year period (2011–2014). AERONET fluxes are validated with ground- and satellite-based flux measurements. To the best of our knowledge this is the first time that AERONET fluxes are validated at the top of the atmosphere. Products such as the aerosol optical depth (AOD), the fraction fine mode to total AOD, the particle size distribution, the sphericity, the radiative forcing and the radiative forcing efficiency show a clear annual cycle. The main drivers of the observed annual cycles are mineral dust outbreaks in summer and the transport of European continental aerosols in spring. A NE–SW gradient is observed on 6 parameters (3 extensive and 3 intensive) out of the 18 discussed in the paper. The NE–SW gradient of the AOD, the Ångström exponent, the coarse mode volume concentration, the sphericity and the radiative forcing at the surface are related to mineral dust outbreaks, while the NE–SW gradient of the coarse mode volume median radius is related to the decreasing influence of European continental aerosols along the NE–SW axis. The fact that two thirds of the parameters discussed in the paper do not present a NE–SW gradient is partly explained by two relevant findings: (1) a homogeneous spatial distribution of the fine particle loads over the three sites in spite of the distances between the sites and the differences in local sources, and (2) low values and the absence of spectral dependency of the absorption found in the southwesternmost site.

ACPD

doi:10.5194/acp-2015-823

1 Introduction

Climate change projections identify the Mediterranean region as a climatologically sensitive area especially vulnerable to global change (Giorgi, 2006; Giorgi and Lionello, 2008). General and regional climate models simulate for the Mediterranean Basin significant changes in the water cycle, a substantial precipitation decrease and a temperature increase before the end of the century (Sanchez-Gomez et al., 2009; Mariotti et al., 2015). Atmospheric aerosols are one of the factors that influence climate change through their impact on the radiation budget (Markowicz et al., 2002). Specifically, atmospheric aerosols influence the Earth's energy budget both directly, because they absorb and scatter solar and terrestrial radiation, and indirectly, because they act as cloud condensation nuclei modifying the structure and the properties of clouds (Twomey, 1974; Albrecht, 1989; Pincus and Baker, 1994). How those impacts distribute themselves in space and time over the greater Mediterranean Basin remains an open question (Mallet et al., 2015, this special issue).

The column amount of atmospheric aerosol, quantified by the aerosol optical depth (AOD), has a direct effect on the solar radiation reaching the Earth's surface. An increase or decrease of AOD can result in enhanced or reduced solar radiation, an effect that Norris and Wild (2007) called solar "brightening" and "dimming", respectively. For that reason the AOD is often used to quantify the aerosol impact on the solar radiation. Numerous studies documenting the spatial variability of the AOD over the Mediterranean Basin are based on long time series of satellite-based observations (Barnaba and Gobbi, 2004; Papadimas et al., 2008; Nabat et al., 2012, 2013, among others) and in a lesser extent on ground-based remote sensing observations (Mallet et al., 2013; Lyamani et al., 2015, among others). The temporal variability of the AOD over the whole Mediterranean Basin has been assessed for the first time by Papadimas et al. (2008) with the AOD at the wavelength of 550 nm and the fraction of fine mode to total AOD products (both over land and ocean) of the Moderate Resolution Imaging Spectroradiometer (MODIS) instrument during the period 2000–2006.

ACPD
doi:10.5194/acp-2015-823

Although the AOD is a key parameter to understand the variability of the aerosol impact on the Earth's energy budget, its analysis is not enough to assess this variability at the scale of the Mediterranean Basin because of the great complexity of the aerosol composition and distribution over the Basin. Bounded to the North by the European continent and to the South by the African continent, the Basin atmosphere is largely affected by maritime aerosols, urban/industrial aerosols from European and North African urban areas and mineral dust from North African arid areas. Anthropogenic particles emitted from ship traffic are also present all-year round while biomass burning aerosols from forest fires from both European and African continents are limited to the summer season. A detailed list of long term analyses or case studies about one or several types of those aerosols can be found in Mallet et al. (2015, this special issue). All those aerosol types have very different optical, microphysical and radiative properties. Consequently, in addition to the AOD, other parameters like the absorption properties, the size of the particles, their shape, etc. are needed to assess the variability of the aerosol impact on the Earth's energy budget at the scale of the Mediterranean Basin.

In this study we perform a seasonal analysis of the aerosol optical, microphysical and radiative columnar properties at two regional background insular sites in Ersa (Corsica, France) and Palma de Mallorca (Mallorca, Spain) over a four-year period (2011–2014). By complementing this dataset with a few months of measurements in the remote island of Alborán (Spain) we obtain the gradient of the aerosol properties on a northeast–southwest (NE–SW) axis in the middle of the western Mediterranean Basin (WMB). The dataset is exclusively composed of AERONET (Aerosol Robotic Network; http://aeronet.gsfc) products. Insular sites were selected in order to minimize the influence of local, non-natural aerosols. The choice of the WMB was motivated by the ChArMEx (the Chemistry-Aerosol Mediterranean Experiment, http://charmex.lsce.ipsl.fr/) program. ChArMEx is a collaborative research program federating international activities to investigate Mediterranean regional chemistry-climate interactions. One of the goals of ChArMEx is precisely to improve our knowledge of

ACPD
doi:10.5194/acp-2015-823

the aerosols over the Mediterranean Basin (Dulac et al., 2014). In its implementation strategy ChArMEx proposes Enhanced Observation Periods (EOP) to study the daily to seasonal scale variability of several parameters measured at several sites and to monitor East–West and North–South gradients over a period of 2–3 years. The AERONET sun-photometer from Ersa was deployed in that framework.

Section 2 of the paper presents the three sites, the dataset and details all the AERONET products used in the paper and their associated accuracy. A general description of the atmospheric dynamics in the WMB is given in Sect. 3.1. The geographical and atmospheric conditions as well as the aerosol loading specific to each of the three sites are detailed in Sect. 3.2. A first comparison between the three sites is made in Sect. 4.1 in terms of monthly variations of the total AOD, the Ångström exponent, the fraction fine mode to total AOD and the sphericity. The seasonal variability of the aerosol absorption optical depth, the absorption Ångström exponent, the particle volume size distribution, the refractive index, the single scattering albedo and the asymmetry factor is assessed in Sects. 4.2–4.4. In order to go one step further and to analyze also the AERONET products of aerosol radiative forcing, we first validate the fluxes estimated by AERONET with ground- and satellite-based flux measurements. The flux validation and the monthly variations of the aerosol radiative forcing and of the aerosol radiative forcing efficiency at the three sites are presented in Sect. 4.5. Finally a discussion is proposed in Sect. 5 on the relationship between the NE–SW gradients observed and the extensive/intensive aerosol properties.

2 Sites and instrumentation

2.1 Sites

The sites selected for this analysis had to fulfill the following criteria: to be located in the WMB, to be insular sites in order to be representative of aerosol regional background conditions, to be approximately aligned on a North–South axis and to have

ACPD
doi:10.5194/acp-2015-823

a recent long-term database (> 2 years). At the same time we wanted to take advantage of the ChArMEx EOP (2–3 years) in the framework of which a supersite was installed at the northern tip of Corsica Island (France), in Ersa (Lambert et al., 2011; Dulac et al., 2014). In that site, situated at 43.00° N, 9.36° W, 80 m a.s.l., an AERONET sun-photometer is operated since June 2008. According to the AERONET Data Display Interface and applying the above mentioned criteria the second site that was selected is Palma de Mallorca in the Balearic Islands (Spain) situated at 39.55° N, 2.62° E, 10 m a.s.l., and operated since August 2011. Both sites are on a NE–SW axis, approximately 670 km apart. A third site considered for comparison is Alborán (Spain, 35.94° N, 3.04° W, 15 m a.s.l.) situated east of Gibraltar midway between the Spanish and the Moroccan coasts. There, an AERONET sun-photometer was operated for a rather short period of time, between June 2011 and January 2012, thanks to a collaboration between the Atmospheric Physic Group of the University of Granada and the Royal Institute and Observatory of the Spanish Navy. Indeed all three sites, reported in Fig. 1, fall onto a quasi-perfect NE–SW straight line and Palma, situated in the middle, is equidistant (∼ 650 km) to both Ersa and Alborán.

2.2 AERONET sun-photometers and products

AERONET is a federated network of ground-based sun-photometers (Holben et al., 1998) which retrieves global aerosol columnar properties. Along with aerosol optical depths at several wavelengths λ, AOD_λ, the AOD products are the Ångström exponent (AE) between pairs of wavelengths, the precipitable water vapor and the total, fine and coarse mode AOD at 500 nm derived from the Spectral Deconvolution Algorithm (SDA, O'Neill et al., 2001, 2003) from which the fine/coarse mode fractions can be calculated.

ACPD
doi:10.5194/acp-2015-823

The AE calculated between two wavelengths λ_1 and λ_2, $AE_{\lambda_1-\lambda_2}$, is defined as

$$AE_{\lambda_1-\lambda_2} = -\frac{\ln\left[\frac{AOD_{\lambda_1}}{AOD_{\lambda_2}}\right]}{\ln\left[\frac{\lambda_1}{\lambda_2}\right]} \quad (1)$$

Further AERONET inversion data products include volume size distribution, the spectral complex refractive index (real and imaginary), the spectral aerosol absorption optical depth, the spectral single scattering albedo, the spectral asymmetry factor, the spectral phase function and the sphericity, i.e. the volume fraction of spherical particles (Dubovik et al., 2000a, 2006; Sinyuk et al., 2007). A series of assumptions are made to perform the inversion of those parameters. They can be found at http://aeronet.gsfc.nasa.gov/new_web/Documents/Inversion_products_V2.pdf. All the inversion products spectrally resolved are given at 440, 675, 870 and 1020 nm, the wavelengths at which the almucantar scans are performed.

The data shown in this work are based on AERONET level 2.0, cloud-screened and quality-assured data (Smirnov et al., 2000) inverted with the AERONET Version 2.0 retrieval algorithm (Holben et al., 2006). In practice the main differences between Version 1.0 and Version 2.0 are the additional criteria applied in Version 2.0 on: the solar zenith angle (SZA $> 50^\circ$ for all products) and the AOD at 440 nm (> 0.4 for the single scattering albedo and the real and the imaginary parts of the refractive index; > 0.2 for the sphericity). The accuracy of AERONET Version 2.0, level 2.0 inversion products is evaluated and discussed in Dubovik et al. (2000b, 2002b) and the additional criteria for Version 2.0 retrieval in Holben et al. (2006). The accuracy of some products has been estimated with numerical sensitivity tests for different aerosol types, namely water-soluble, dust and biomass burning (Dubovik et al., 2000b).

- The estimated accuracy of AOD_λ is ±0.02 (Eck et al., 1999).
- The accuracy of the Ångström exponent is estimated to be ± 0.25 for $AOD_{440} \geq 0.1$ and of the order of 50 % for $AOD_{440} < 0.1$ (Toledano et al., 2007).

ACPD
doi:10.5194/acp-2015-823

- The accuracy of the volume size distribution is estimated to be: 15 % for water-soluble, 35 % for dust and 25 % for biomass burning in the intermediate particle size range ($0.1 \leq r \leq 7\,\mu m$); and 15–100 % for water-soluble, 35–100 % for dust and 25–100 % for biomass burning for the edges ($0.05 \leq r < 0.1\,\mu m$ and $7 < r \leq 15\,\mu m$).

- The accuracy of the real (imaginary in %) part of the refractive index is estimated to be ±0.025 (50 %) for $AOD_{440} > 0.2$ for water-soluble and ±0.04 (50 and 30 %, respectively) for $AOD_{440} \geq 0.5$ for dust and biomass burning.

- The retrieved aerosol absorption optical depth at wavelength λ ($AAOD_\lambda$) has an accuracy of ±0.01 at $\lambda \geq 440$ nm.

- The accuracy of the single scattering albedo at wavelength λ (SSA_λ) is estimated to be ±0.03 for $AOD_{440} > 0.2$ for water-soluble and for $AOD_{440} \geq 0.5$ for dust and biomass burning.

- The asymmetry factor at wavelength λ (g_λ) uncertainty ranges between ±0.03 and ±0.08 for pollution and biomass burning aerosols and is ±0.04 for desert dust particles.

It is important to note that some products such as the AAOD, the real and the imaginary parts of the refractive index and the SSA are retrieved only if the criteria $AOD_{440} > 0.4$ is fulfilled. Such aerosol loads are generally associated to desert dust events.

Other parameters of interest for this work delivered by the AERONET inversion algorithm are the instantaneous solar broadband (0.2–4 µm) downward and upward fluxes, as well as the aerosol radiative forcing and radiative forcing efficiency at the surface and at the top of the atmosphere. A brief description on how the fluxes are calculated is given at http://aeronet.gsfc.nasa.gov/new_web/Documents/Inversion_products_V2.pdf. The gaseous absorption is calculated by the GAME (Global Atmospheric Model) radiative transfer model (Dubuisson et al., 1996).

ACPD
doi:10.5194/acp-2015-823

Table 1 indicates the availability of AERONET inversions at the three sites during the period 2011–2014. At Ersa almost all months are represented at least three times (except November and December), while at Palma all months are represented at least twice (except the first four months of the year).

3 Atmospheric dynamics

3.1 Atmospheric dynamics of the WMB

The Mediterranean region features an almost enclosed sea surrounded by very urbanized littorals and important mountain barriers. The gaps between the major mountainous regions act as channels for the air mass transport toward the Mediterranean Basin which constitutes a crossroads of air masses carrying aerosols from different natural and anthropogenic sources (Lelieveld et al., 2002). In particular in the WMB those channels are the Strait of Gibraltar and the Ebro Valley in Spain, the Rhône Valley in France and the Po valley in Italy. The atmospheric dynamics of the WMB is mainly governed by the extended subtropical anticyclone of the Atlantic (Azores anticyclone) and can be roughly divided into cold and warm periods (Maheras et al., 1999; Kallos et al., 2007), respectively associated with low and high aerosol loads. A significant amount of literature exists about the relationship between the synoptic conditions in the Mediterranean Basin and the occurrence of aerosol episodes (e.g. Gangoiti et al., 2001; Lelieveld et al., 2002; Kallos et al., 2007, and papers cited therein; Papadimas et al., 2008; Gkikas et al., 2012).

In winter and part of spring, the Azores anticyclone presents its lowest intensity and usually stays west of the WMB (Millán et al., 1997). Weak gradient anticyclonic conditions in are recurrent over the WMB and favor the stagnation of pollutants near populated and industrialized areas around the Basin. The thermal inversions associated to such anticyclonic conditions and the local breezes that may be activated by solar radiation help the pollutants to disperse over the Basin. Winter is also the time when the

ACPD
doi:10.5194/acp-2015-823

Azores anticyclone leaves room to an anticyclone that may form over the Bay of Biscay. It is a favorable situation for the entry of Atlantic air masses through the Gulf of Lion to the WMB allowing to the renewal of air masses and the removal of aerosols that may have accumulated over the Basin (Escudero et al., 2007). Moreover the aerosols are also removed by scavenging, which is the strongest removal mechanism (Pruppacher and Klett, 1997), due to the large precipitation amounts.

In summer, the Azores anticyclone is strengthened and its eastern edge enters the WMB between the Iberian and the Italian peninsulas, whereas thermal lows develop over the Iberian Peninsula and the Sahara region (Millán et al., 1997). The summer months in the region are characterized by the absence of large-scale forcing and the predominance of mesoscale circulations. In particular, as far as the Iberian Peninsula is concerned, the interaction of the sea–land and mountain-induced breezes, the strong orography, the convergence of surface winds from the coastal areas towards the central plateau and the strong levels of subsidence over the WMB results in the re-circulation of air masses and the consequent ageing and accumulation of pollutants (Millán et al., 1997; Pérez et al., 2004; Sicard et al., 2006). Furthermore, additional factors come into play such as low precipitation, high photochemistry that boosts the formation of secondary organic aerosols and the increased convective dynamics that favors resuspension. Summer is also a period favorable to the transport of aerosols such as desert dust and forest fires towards the Basin (Bergametti et al., 1992). The annual amount of desert dust exported to the Basin is controlled by the large-scale North Atlantic Oscillation (NAO; Papadimas et al., 2008; Pey et al., 2013) which also partly controls the number of fires around the Basin: during period of high NAO index (defined by Hurrel, 1995), drier conditions prevail over southern Europe, the Mediterranean Sea, and northern Africa (Papadimas et al., 2008).

3.2 Peculiarity of each of the three sites

Corsica, where the Ersa site is located, is an 80 km × 180 km island situated in the northern part of the WMB. It has the highest mountains and the largest number of

ACPD
doi:10.5194/acp-2015-823

rivers than any Mediterranean island. The highest peak reaches 2710 m and there are about twenty other summits higher than 2000 m. The northen tip of the island is at about 160 km from the coast of southern continental France and at about 80 km from the coast of Italy. The dominant wind directions are W and E–SE (Lambert et al., 2011). The site is perfectly suited for regional background studies since it is not impacted by any type of local anthropogenic aerosol. There is relatively few aerosol measurements over Corsica in the scientific literature at present despite the recurrent high summer pollution peaks and intense rainfalls observed in the island in the last few years (Lambert and Argence, 2007). However, the French scientific community has started the installation of a multi-site instrumented platform, called CORSiCA (Corsican Observatory for Research and Studies on Climate and Atmosphere–ocean environment), dedicated to oceanographic and atmospheric studies in the framework of the HyMeX (Hydrological cycle in the Mediterranean Experiment) and ChArMEx projects (Lambert et al., 2011). In the framework of ChArMEx Léon et al. (2015, this special issue) presented the aerosol vertical distribution at Ersa obtained from lidar measurements during more than one year. In that study less than 10 % of the observation days were affected by desert dust events. AOD_{355} was estimated to be 0.61 for dust and 0.71 for pollution building up in the Gulf of Genova. Carbonaceous aerosols were highlighted as the main driver of the aerosol optical properties in summer (Sciare et al., 2014).

The island of Mallorca is approximately 2.5 times smaller than Corsica in surface. The mountainous chain of the island, the Sierra de Tramuntana, is situated in the northwestern part and its highest peak reaches 1445 m. The AERONET sun-photometer is situated at the airport of the capital, Palma de Mallorca (~ 420 000 inhabitants), approximately 8 km east of the city center and the harbor area. The winds are driven by the topographic effects of the Sierra de Tramuntana chain. The dominant wind directions observed close to the city center are SW and NE to which a NW component adds in winter (Pey et al., 2009). There are also relatively few aerosol measurements over Mallorca in the scientific literature. In average 20 % of the days $year^{-1}$ are affected by desert dust events (Pey et al., 2009). The amount of carbonaceous aerosols observed

ACPD
doi:10.5194/acp-2015-823

by the same authors, found in the same range that those for other suburban sites in Spain, suggests an important regional contribution of such aerosols.

The Alborán island is a tiny (7 ha), totally flat island situated 50 km north of the Moroccan coast and 90 km south of the Spanish coast. There is no local anthropogenic emission source on and near the island, except for an important shipping route at the north of it (www.marinetraffic.com). The only aerosol measurements performed in Alborán are those presented in this work. They are extensively discussed in Lyamani et al. (2015) and Valenzuela et al. (2015). During the period of June 2011–January 2012, 40 % of the days were dominated by pure maritime aerosols and 31 % of the days were dominated by desert dust (Lyamani et al., 2015; Valenzuela et al., 2015). During the dust events, Valenzuela et al. (2015) stresses that the aerosol properties are clearly different from pure mineral dust and that most of the desert dust intrusions over Alborán can be described as a mixture of dust and anthropogenic fine absorbing particles independently of the dust source area.

The frequency of desert dust events referenced here (< 10, 20 and 31 % at Ersa, Palma and Alborán, respectively) are in agreement with the long-term study over the whole Mediterranean Basin made by Pey et al. (2013).

4 Seasonal and annual variability of aerosol properties

4.1 AOD, AE and fine mode contribution

Figure 2 shows the hourly variation of the AOD at 440 nm at the three sites. This figure aims at showing the representativeness of the dataset at Ersa and Palma. The number of points, *N*, at each site is reported in the figure. One sees that Ersa and Palma have at least 2 years of data within the 4 year period and that Alborán has a single sample of data between June 2011 and January 2012. Both at Ersa and Palma the AOD shows a marked annual cycle with maxima in spring and summer in Ersa and in summer in Palma, and minima in December and January at both stations. The AOD reaches peak

ACPD
doi:10.5194/acp-2015-823

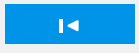

values as high as 1.82 at Ersa and 1.12 at Palma. The episodes with high aerosol loads (AOD > 0.5) at Alborán are also detected in Palma with less intensity and less frequency. There is no clear correlation with Ersa.

The monthly mean values of AOD_{440}, $AE_{440-870}$, the fine mode AOD_{440} and of the sphericity are shown in Fig. 3. The seasonal mean values of AOD_{440} and $AE_{440-870}$ are given in Table 2. AOD_{440} shows a clear annual cycle at Ersa and Palma. Maxima of 0.21 in Ersa and 0.25 in Palma are observed in July. Those maxima are due to mineral dust outbreaks, being these events more frequent in summer. The decreasing trend in AOD during the autumn months (SON) is identical at all three sites. The spring AOD is lower in Palma than in Ersa, while it is the opposite in summer/autumn. The background AOD in spring in Ersa is dominated by small particles located in the marine boundary layer, present throughout the year (Sciare et al., 2014), while at Palma the predominance of the Atlantic advection meteorological scenario in spring leads to the renovation of air masses at regional scale through the Gulf of Lion and to the cleaning of the atmosphere (Escudero et al., 2007). AOD_{440} shows also a NE–SW gradient during the summer months. The summer mean AOD_{440} is (±standard deviation) 0.18 ± 0.10, 0.23 ± 0.12 and 0.27 ± 0.14 in Ersa, Palma and Alborán, respectively, while the winter averages vary between 0.07 and 0.09. The NE–SW gradient observed in summer is reproduced on the annual mean (0.16 ± 0.10, 0.18 ± 0.12 and 0.20 ± 0.13 in Ersa, Palma and Alborán, respectively, and listed in that order from NE to SW in the rest of the paper) which indicates that the summer values contribute significantly to the annual means.

The monthly $AE_{440-870}$ (Fig. 3b) shows different seasonal patterns at the three sites. In Ersa it slightly increases in winter/spring (from 0.98 in January) to reach a maximum value of 1.56 in September. In Palma, it oscillates between 0.84 (March) and 1.34 (September) without any significant trend. The slightly higher values in Ersa compared to Palma indicate the presence of finer particles at Ersa throughout the year. At Alborán the AE is lower, especially in June and August (0.43–0.45) owing to the high African dust load of the Alborán Sea region in summer (Moulin et al., 1998). There is also

ACPD
doi:10.5194/acp-2015-823

a clear NE–SW gradient between the 3 stations on the annual means (1.38 ± 0.48, 1.14 ± 0.46, 0.81 ± 0.40), especially strong in summer (1.44 ± 0.47, 1.14 ± 0.47, 0.61 ± 0.33). The coarse mode fraction (not shown, see Sicard et al., 2014) looks reversely correlated to the AE: it decreases in Ersa in winter/spring and reaches a minimum in July, while no marked trend is observed at Palma. The coarse mode fraction also shows a NE–SW gradient more evident in summer (0.26, 0.42, 0.61) than on the annual means. Here again this result clearly evidences the predominant contribution of large particles in Alborán during the summer months which decreases quasi-linearly as we move to Palma and then Ersa.

In order to see the contribution of the fine mode particles we have plotted the fine mode AOD_{440}, AOD^{f}_{440}, in Fig. 3c. Except for two months (March and April) the annual cycles at both Ersa and Palma are similar in shape and magnitude. In Alborán, the monthly AOD^{f}_{440} presents larger fluctuations but is similar to the results at the other two stations. Maxima are found in summer (0.13±0.09 in Ersa, 0.12±0.07 in Palma and 0.09 ± 0.04 in Alborán). Because of those similarities no NE–SW gradient is observed on AOD^{f}_{440}. Our findings, in agreement with Lyamani et al. (2015), suggest a homogeneous spatial distribution of the fine particle loads over the three sites in spite of the distances between the sites and the differences in local sources. In March and April AOD^{f}_{440} is more than double in Ersa than in Palma. The maps of AOD per aerosol type from Barnaba and Gobbi (2004) suggest a contribution of aerosols of continental origin already in spring over Corsica and not before summer over the Balearic Islands. An interesting conclusion so far is that the seasonal variations of the fine particle load are quite homogeneous over the WMB in spite of heterogeneous origins (of the fine particles): mostly European/continental at the north of the Basin and from North African urban/industrial areas (Rodríguez et al., 2011) and/or from ship emissions (Valenzuela et al., 2015) at the south.

Finally the sphericity (Fig. 3d) could be retrieved for a few months of the year only because it requires that the sun-photometer measurements cover the scattering angle range from aureole to > 120° which is not possible for large solar zenith angles dur-

ACPD
doi:10.5194/acp-2015-823

ing winter months. The sphericity presents huge variations resulting in large monthly standard deviations (see Table 2). As expected it is strongly correlated to desert dust intrusions and therefore presents a clear summer NE–SW gradient. It reaches minima in summer of 57 ± 45, 41 ± 41 and 25 ± 32 % in Ersa, Palma and Alborán, respectively.

4.2 AAOD and AAE

The seasonal variations of the spectral dependency of the aerosol absorption optical depth are shown in the top part of Fig. 4, while the annual means of the AAOD spectra are shown in the bottom part of Fig. 4. Seasonal mean values are given in Table 2. Bergstrom et al. (2007) reported that the spectral AAOD for aerosols representing the major absorbing aerosol types (pollution, biomass burning, desert dust and mixtures) decreases with wavelength and can be approximated with a power-law wavelength dependence, the absorption Ångström exponent (AAE) which can be calculated between two wavelengths λ_1 and λ_2, $\mathrm{AAE}_{\lambda_1-\lambda_2}$, as:

$$\mathrm{AAE}_{\lambda_1-\lambda_2} = -\frac{\ln\left[\frac{\mathrm{AAOD}_{\lambda_1}}{\mathrm{AAOD}_{\lambda_2}}\right]}{\ln\left[\frac{\lambda_1}{\lambda_2}\right]} \quad (2)$$

The range of values of AAE provides useful information on shortwave absorption produced by different types of aerosols, namely black carbon (BC), organic carbonaceous matter, and mineral dust (Russell et al., 2010). However, recently, Mallet et al. (2013) highlighted the difficulties in attributing AAE larger than 1, the value for pure BC, to organic species (and/or mineral dust) or to coated BC since they all produce AAE > 1 (Lack and Cappa, 2010).

In both Ersa and Palma the AAOD decreases with increasing wavelength. The annual AAOD_{440} is 0.023 ± 0.018 in Ersa and 0.040 ± 0.020 in Palma. The associated $\mathrm{AAE}_{440-870}$ is 1.66 ± 0.66 and 1.88 ± 0.53, respectively. The box-and-whisker plots of the AAOD indicate a higher spread of the values at 440 nm than at the other wave-

ACPD
doi:10.5194/acp-2015-823

lengths, as well as a general good symmetry of the point distribution around the mean (mean ≈ median). Palma is logically characterized by a larger AAOD than Ersa because of the nearby city and harbor of Palma de Mallorca and because of the higher frequency of dust events. The summetime average of $AAOD_{440}$ in Ersa (0.018) is within the error bar of the value found by Mishra et al. (2014, this special issue; 0.020) at the same site from a larger dataset of AERONET observations. It is however lower than the average value given in Mallet et al. (2013) for the WMB calculated at sites caracterized mostly as urban and dusty. The AAOD spectra at both sites are similar in magnitude and shape to the measurements made during PRIDE (Puerto Rico Dust Experiment, 2000; aerosols: Saharan dust) and ACE-Asia (Aerosol Characterization Experiment-Asia, 2001; aerosols: Asian dust, urban and industrialized) (Bergstrom et al., 2007; Russell et al., 2010). The AAE in both sites are higher than the mean values for the WMB (1.32) and for urban sites (1.31) but are smaller than the mean value of 1.96 for dusty sites (Mallet al., 2013). It is worth remembering that the AERONET level 2.0 products retain only cases with $AOD_{440} > 0.4$ for estimating AAOD. This condition, applied in clean sites such as Ersa and Palma, yields AAOD strongly influenced by mineral dust and also, but very seldomly, by pollution. It results that the AAE values found are mostly representative of mineral dust and not so much of organic particles. Indeed the annual mean values of AAE fall within the range 1.5–2, in which the AAE at different wavelength pairs vary in the dusty site of Solar Village, Saudi Arabia (Russell et al., 2010). The few points available in Alborán ($N = 15$) give a summer mean $AAOD_{440}$ of 0.016 ± 0.010 and an AOD spectra almost without any wavelength dependency (AAE $= 1.05 \pm 0.26$). A further inspection of the 15 cases indicates that they all correpond to dust events. In 12 cases (80 %) the airmasses arriving in Alborán are from the southwest quadrant. The AAOD value is the lowest of the whole Mediterranean Basin if we compare with the results from Mallet et al. (2013) given for AERONET sites all around the Mediterranean Basin and in which the minimum (0.023) is found precisely in Ersa. The AAE, nearly equal to 1, is totally surprising since the predominant aerosol is expected to be mineral dust. Curiously the summer value of 1.05 in Alborán

ACPD
doi:10.5194/acp-2015-823

is close to 1.12 observed during TARFOX (Tropospheric Aerosol Radiative Forcing Observational Experiment, 1996; location: US Atlantic coast) and 1.05 observed during ICARTT (International Consortium for Atmospheric Research on Transport and Transformation, 2004; location: New England Atlantic coast) (Bergstrom et al., 2007; Russell et al., 2010). Both field campaigns have the peculiarity of being shipborne campaings. All in all, those AERONET retrievals allow to make the hypothesis that, although detected in small amount (low AAOD), BC and/or soot originated from North African urban/industrial areas (Rodríguez et al., 2011) and/or from both the harbor of Algeciras and vessel traffic near the Strait of Gibraltar drive the absorbing spectral behavior in Alborán. The emissions of the two latter have been quantified in the Bay of Algeciras by Pandolfi et al. (2011). Further research (and probably measurements) is (would be) needed to understand the low spectral dependency of AAOD in Alborán.

4.3 Volume size distribution and refractive index

Figure 5 shows the seasonal variability of the aerosol particle size distribution at the three sites. Seasonal mean values are given in Table 3. The annual volume concentration values (varying between 0.017 and 0.021 $\mu m^3\ \mu m^{-2}$ for the fine mode and between 0.027 and 0.062 $\mu m^3\ \mu m^{-2}$ for the coarse mode) at all three sites are typical of maritime (Smirnov et al., 2002) and/or background/rural (Omar et al., 2005) environments. The annual values at Palma are very similar to the mean size distribution averaged over several sites in the WMB by Mallet et al. (2013). The winter fine mode volume concentrations are similar at all three sites and vary between 0.009 and 0.012 $\mu m^3\ \mu m^{-2}$. In spring the fine mode volume concentration more than doubles (w.r.t. winter) in Ersa while it is stable in Palma. This behavior is reflected on AOD^{f}_{440} (Fig. 3c) which doubles from winter to spring in Ersa because of the contribution of aerosols of continental origin already in spring over Corsica and not before summer over the Balearic Islands. The domination of large particles (mostly mineral dust) is particularly remarkable during the summer period at all three sites, and is still clearly visible in autumn in Palma and Alborán. The NE–SW gradient observed on the summer coarse mode fraction

ACPD
doi:10.5194/acp-2015-823

commented earlier (0.26, 0.42, 0.61) is also observed on the coarse mode volume concentration (0.032 ± 0.036, 0.063 ± 0.063, $0.083 \pm 0.063\,\mu m^3\,\mu m^{-2}$) and also on the C_V^c/C_V^f ratio (1.7, 2.5, 3.6). The summer coarse mode volume median radii (2.49 ± 0.41, 2.43 ± 0.41, $2.33 \pm 0.45\,\mu m$) falls in the range of values for dusty sites (1.90–2.54 µm; Dubovik et al., 2002b) and are in agreement with the average value of 2.34 µm for the WMB found by Mallet et al. (2013). As commented by Dubovik et al. (2002b) the absence of dynamics between the particle radius and the aerosol loading explains that dust median radii are smaller than those of urban/industrial aerosols. The influence of European pollution decreases along the NE–SW axis and, logically, the coarse mode volume median radius decreases. This result also suggests that the influence of European pollution in the northern WMB (Ersa) is stronger than the influence of North African pollution in the southern WMB (Alborán) in term of particle size.

The seasonal and annual spectral variations of the real and the imaginary part of the refractive index (RRI and IRI, respectively) are shown in Fig. 6 and Fig. 7. Seasonal mean values of RRI_{440} and IRI_{440}, the RRI and IRI at 440 nm, respectively, are given in Table 3. RRI_{440} has an annual mean value of 1.45 ± 0.04 in Ersa and 1.43 ± 0.06 in Palma. Those values are on the order of magnitude of the values found by Mallet et al. (2013) at various sites around the Mediterranean Basin and they are in the upper limit of urban/industrial aerosols (1.33–1.45) and lower than "pure" dust (1.48–1.56; Dubovik et al., 2002b). Airborne measurements of particle size distributions and aerosol absorption coefficients during the SAMUM (Saharan Mineral Dust Experiment) campaign allowed to determine the RRI of desert dust with values between 1.55 and 1.56 (Petzold et al., 2009). Figure 6 does not reveal neither a clear NE–SW gradient, nor a significant dependency with the season. The wavelength dependency is slightly stronger in Palma and Alborán than in Ersa. This can be explained by a higher influence of non-spherical particles (mineral dust) over Palma and Alborán, and thus a stronger spectral dependence of the real part of the refractive index (Dubovik et al., 2000b). The box-and-whisker plots show a high spread of RRI at all wavelengths in both Ersa

ACPD
doi:10.5194/acp-2015-823

and Palma. Minima and maxima are found below 1.35 and above 1.55, respectively, spanning a large range of values corresponding to different aerosol types.

IRI_{440} (Fig. 7, Table 3) has an annual mean value of $3.1 \pm 1.3 \times 10^{-3}$ at Ersa and $4.7 \pm 1.8 \times 10^{-3}$ at Palma. While IRI_{440} is different at both sites, the rest of the spectral IRI is similar at both sites. The annual IRI_{440} are in the lower limit of the values found by Mallet et al. (2013) at various sites around the Mediterranean Basin ($3.5–11.9 \times 10^{-3}$) where the minimum (3.5×10^{-3}) was observed at the Italian Island of Lampedusa. During the TARFOX campaign values of $1–8 \times 10^{-3}$ were found off the US Atlantic coast in horizontal layers of distinct aerosol refractive indices using a retrieval based on aerosol in-situ size distribution and remote sensing measurements (Redemann et al., 2000). During SAMUM Petzold et al. (2009) retrieved values of desert dust RRI at 450 nm of $3.1–5.2 \times 10^{-3}$. At both Ersa and Palma the seasonal IRI decreases with increasing wavelengths. From 440 to 675 nm the decrease in IRI is stronger at Palma (especially in summer where IRI decreases by a factor larger than (2) than at Ersa. As the imaginary part of the refractive index is driven by iron oxide content (especially hematite), it results in a higher IRI at shorter wavelengths during episodes with high dust concentrations (Moosmüller et al., 2009). However mineral dust is not the only aerosol type which could explain the IRI spectral behavior: brown carbon (BrC), a class of light-absorbing carbonaceous material, has also an IRI that increases towards shorter visible and ultraviolet wavelengths (Moosmüller et al., 2009). We conclude that the differences in the IRI_{440} values and in the behavior of the IRI spectra are due to a higher influence of mineral dust and/or BrC in Palma. Pey et al. (2009) estimated from in-situ measurements in the city of Palma de Mallorca the annual contribution of mineral dust and organic matter on the total aerosol mass concentration to be 29 and 17 %, respectively. This result points out that mineral dust might be the main driver of the IRI_{440} values and the IRI spectra behavior found in Palma. Here again the box-and-whisker plots (bottom plots of Fig. 7) show a high spread of IRI at all wavelengths in both Ersa and Palma with minima and maxima below 1×10^{-3} and above 8×10^{-3}, respectively.

ACPD
doi:10.5194/acp-2015-823

The summer IRI at Alborán is totally different from the other two sites: it is rather low, 1.14×10^{-3} in average, and wavelength-independent. The absence of wavelength dependency points out towards the presence of BC and/or soot and supports the hypothesis of an anthropogenic influenced mineral dust (we recall that all the 15 cases in Alborán correspond to dust events, see Sect. 4.2). This hypothesis, already formulated by Müller et al. (2009) who determined separately mineral dust and soot absorption coefficients near the source during SAMUM, is confirmed by the results from Valenzuela et al. (2015) that state that most of the desert dust intrusions over Alborán can be described as a mixture of dust and anthropogenic fine absorbing particles (BC and/or soot) independently of the dust source area. In our opinion two major and interesting questions remain opened: why the absorption properties of the long-range transport aerosol in Alborán are observed neither in Palma, nor in Ersa? What are the processes which inhibits the BC and/or soot absorption properties during the transport to the northern part of the WMB?

4.4 Single scattering albedo and asymmetry factor

The single scattering albedo is the ratio of aerosol scattering to total extinction (i.e. scattering + absorption) that provides some information on the aerosol absorption properties. It is useful to relate the AAOD to the AOD:

$$\mathrm{AAOD}_\lambda = (1 - \mathrm{SSA}_\lambda)\,\mathrm{AOD}_\lambda \quad (3)$$

The asymmetry factor (g) represents a measure of the preferred scattering direction and varies between −1 (only backward-scattering at 180°) and +1 (only forward-scattering at 0°). The SSA and asymmetry factor are of special interest for radiative transfer studies. The seasonal and annual spectral variations of SSA and g are shown in Figs. 8 and 9. Seasonal mean values of SSA_{440} and g_{440}, the SSA and asymmetry factor at 440 nm, respectively, are given in Table 4. In average the three sites appear as "moderately" absorbing with annual SSA_{440} varying between 0.92 and 0.97, even though minima are observed around 0.89 and 0.86 at Ersa and Palma, respectively. In

ACPD
doi:10.5194/acp-2015-823

agreement with our previous results (higher $AAOD_{440}$ at Palma than at Ersa) we find lower SSA at Palma compared to Ersa at all wavelengths but especially at 440 nm. The annual SSA_{440} is 0.92 ± 0.03 at Palma while it is 0.96 ± 0.02 at Ersa. If we compare the SSA spectra with other stations around the Mediterranean Basin (Mallet et al., 2013) we find that the SSA spectra at Ersa has a shape identical to the average of AERONET sites in the WMB but higher values (an difference of approximately +0.04) and that the SSA spectra at Palma has a shape identical to the dusty AERONET sites. The climatological SSA spectra obtained worldwide by Dubovik et al. (2002b) for urban/industrial aerosols, biomass burning and desert dust has been plotted by Russell et al. (2010). The spectral behavior of those three aerosol types is: SSA_λ decreases with increasing wavelengths for urban/industrial aerosols and biomass burning, and increases with increasing wavelengths for desert dust. Maritime aerosols have large (> 0.97), wavelength-independent SSA (Dubovik et al., 2002b). A monotonous (here increasing) SSA spectra is only observed at Palma during the summer season and corresponds to the signature of mineral dust. During the rest of the seasons available in our statistics (summer, autumn and spring in Ersa and autumn in Palma), SSA_λ increases from 440 to 675 nm and decreases afterwards. This behavior does not fit with any of those of the climatology just mentioned and are therefore representative of a mixture of aerosols, namely urban/industrial aerosols and mineral dust. In Alborán, as expected from our previous results (low AAOD and IRI), SSA is high (summer mean: 0.97 ± 0.02) and shows a poor wavelength dependency. Here again the values of SSA and the shape of its spectra are representative of a mixture of aerosols. In view of the results from Dubovik et al. (2002b) and Russell et al. (2010), such a mixture could be quantitatively produced by a mixture of urban/industrial aerosols (e.g. from Goddard Space Flight Center; $SSA_{440} = 0.98$, SSA_λ decreases with increasing wavelengths) and mineral dust (e.g. from Bahrain, Persian Gulf; $SSA_{440} = 0.92$, SSA_λ increases with increasing wavelengths). For comparison Denjean et al. (2015, this special issue) found SSA_{530} ranging from 0.90 to 1.00 ± 0.04 in mineral dust layers in the WMB during summer 2013. Last, it is worth noting that the SSA spectra found in our studies at Alborán

ACPD
doi:10.5194/acp-2015-823

are quite different from the results of Valenzuela et al. (2015) for North Atlantic air masses. Several reasons explain those differences:

- Valenzuela et al. (2015) make use of the Nakajima et al. (1996) retrieval scheme adapted for non-spherical particles (Olmo et al., 2008) while in this study the AERONET retrieval scheme is used (see Sect. 2.2 for references about the AERONET inversion algorithm).
- Nakajima code uses sky radiance measurements in the solar principal plane while AERONET uses almucantar sky radiance measurements.
- By not using the same configuration for the sky radiance measurements, the inversions from Valenzuela are not coincident in time with those of our study and the positions of the aerosol volume sampled are also different.
- AERONET retrieval applies the criteria $AOD_{440} > 0.4$ for retrieving the SSA while Nakajima code does not apply any criteria.
- Despite small standard deviations (< 0.02, see Fig. 8) which indicate good stability of our results, our statistics is based on a small amount of numbers ($N = 15$).
- Previous works (e.g. Alados-Arboledas et al., 2008; Olmo et al., 2008; Valenzuela et al., 2012a) have studied the differences between both the Nakajima and the AERONET retrieval scheme and have found SSA retrieved with the Nakajima code in general lower than with the AERONET code, with a difference of up to 7 %.

Figure 9 shows that the asymmetry factor has a general tendency to decrease with increasing wavelengths. The annual mean values at 440 nm are 0.69 ± 0.03 and 0.70 ± 0.03 at Ersa and Palma, respectively, and minor inter-season variations are observed (Table 4). The decrease for $\lambda > 440$ nm occurs at all wavelengths in Ersa ($g_{1020} = 0.62$) while a slight increase is observed in Palma from 870 to 1020 nm ($g_{1020} = 0.66$). According to Dubovik et al. (2002b) urban/industrial aerosols and desert

ACPD
doi:10.5194/acp-2015-823

dust have a similar g_{440} (0.68–0.73), biomass burning has a g_{440} between 0.64 and 0.69 and strongly decreasing with wavelength and maritime aerosol have a slightly higher g_{440} ($\sim$ 0.75). The similarities between urban/industrial aerosols and desert dust make difficult the identification of a predominant aerosol type from the annual means and spectral variations at Ersa and Palma. According to Lyamani et al. (2006) who compared the asymmetry factor spectra at Granada for dust events and urban/industrial aerosols (European contamination) the decrease of the g spectra with increasing wavelengths is much stronger for urban/industrial aerosols than for mineral dust. This result is also observed by Dubovik et al. (2002b) at urban/industrial sites vs. desert dust sites and indicates that at near-infrared wavelengths ($\lambda > 670$ nm) and at constant AOD the solar radiation scattered to the surface is greater for mineral dust than for urban/industrial aerosols. The stronger spectral variations of g at Ersa are therefore in agreement with the higher influence of aerosols of continental origin at that site. In all cases the spread around the median, which is always close to the mean, is small and indicates a good stability of our results, while outliers are relatively far from the first and third quartile boxes. The summer asymmetry factor at Alborán is higher than at the other two sites ($g_{440} = 0.74 \pm 0.02$) and its spectral variations are similar in shape to that of Palma but slightly stronger ($g_{1020} = 0.68 \pm 0.02$) The g spectra at Alborán is indeed quite similar to that of maritime aerosols ($g_{440} = 0.75$ and $g_{1020} = 0.68 \pm 0.02$) determined in Lanai, Hawaii, by Dubovik et al. (2002b). Valenzuela et al. (2012b) showed that the asymmetry factor at 440 nm measured in Granada (140 km N–NW of Alborán) over a 6 year period during dust events was $\sim$ 0.70. This result indicates that the preferred scattering direction in Alborán may be driven by marine aerosols.

4.5 Solar radiative forcing and forcing efficiency

The AERONET Version 2.0 retrieval provides a set of radiative quantities including spectral downward and upward total fluxes at the surface, diffuse fluxes at the surface, and broadband upward and downward fluxes as well as aerosol radiative forcing (ARF) and aerosol radiative forcing efficiency (ARFE) both at the bottom of atmosphere (BOA)

ACPD
doi:10.5194/acp-2015-823

and at the top of the atmosphere (TOA). The radiative forcing accounts for changes in the solar radiation levels due to changes in the atmospheric constituents. The direct radiative forcing of atmospheric aerosols is defined as the difference in the energy levels between two situations with and without aerosols:

$$\mathrm{ARF}_{\mathrm{BOA}} = \Delta F^{\mathrm{w}}_{\mathrm{BOA}} - \Delta F^{\mathrm{o}}_{\mathrm{BOA}} \quad (4)$$

$$\mathrm{ARF}_{\mathrm{TOA}} = \Delta F^{\mathrm{w}}_{\mathrm{TOA}} - \Delta F^{\mathrm{o}}_{\mathrm{TOA}} \quad (5)$$

where ΔF^{w} and ΔF^{o} are the downward net (downwelling minus upwelling) fluxes with and without aerosols, respectively. With this convention, a negative sign of the ARF implies an aerosol cooling effect and a positive sign an aerosol warming effect, regardless of whether it happens at the BOA or at the TOA. The ARFE is defined as the ratio of ARF per unit of AOD. The ARF analytical definitions used by AERONET (see http://aeronet.gsfc.nasa.gov/new_web/Documents/Inversion_products_V2.pdf) are slightly different than Eqs. (4) and (5):

$$\mathrm{ARF}^{\mathrm{AER}}_{\mathrm{BOA}} = F^{\mathrm{w}\downarrow}_{\mathrm{BOA}} - F^{\mathrm{o}\downarrow}_{\mathrm{BOA}} \quad (6)$$

$$\mathrm{ARF}^{\mathrm{AER}}_{\mathrm{TOA}} = F^{\mathrm{o}\uparrow}_{\mathrm{TOA}} - F^{\mathrm{w}\uparrow}_{\mathrm{TOA}} \quad (7)$$

While Eq. (7) is equivalent to Eq. (5) because the downwelling flux at the TOA is independent of the presence or not of aerosols in the atmosphere ($F^{\mathrm{w}\downarrow}_{\mathrm{TOA}} = F^{\mathrm{o}\downarrow}_{\mathrm{TOA}}$), the use of Eq. (6) yields an overestimation w.r.t. the real value since the upward fluxes with and without aerosols are not taken into account.

Similar to the AERONET retrieval approach, the flux calculations account for the thermal emission, absorption and single and multiple scattering effects using the Discrete Ordinates Radiative Transfer (DISORT) method (Stamnes et al., 1988). The solar broadband fluxes are calculated for SZA between 50 and 80°, by spectral integration in the range from 0.2 to 4.0 µm. The integration of atmospheric gaseous absorption and molecular scattering effects are conducted using the Global Atmospheric Model

ACPD
doi:10.5194/acp-2015-823

(GAME) code (Dubuisson et al., 1996, 2004, 2006). It is worth noting that flux calculations are performed for a multi-layered atmosphere with a gaseous vertical distribution calculated with the US standard atmosphere model and a single fixed aerosol vertical distribution (exponential with aerosols up to a height of 1 km). García et al. (2008) tested different vertical profiles and their sensitivity tests led to differences of less than $1\,W\,m^{-2}$ on the downward solar flux at the BOA. Those differences (~ 0.2–$3\,\%$ w.r.t. the instantaneous ARF) were estimated negligible by the same authors. Detailed information on the radiative transfer module used by the operational AERONET inversion algorithm can be found in García et al. (2011, 2012a, b).

AERONET estimations of the aerosol direct radiative forcing are little used in the literature. Cachorro et al. (2008) used the AERONET ARF estimations to study the impact of an extremely strong desert dust intrusion over the Iberian Peninsula. García et al. (2008) made an intensive validation of AERONET estimations of fluxes and radiative forcings using ground-based measurements from solar databases at 9 stations worldwide. Derimian et al. (2008) used the AERONET estimates of the ARF for mineral dust mixed with biomass burning and for pure mineral dust at M'Bour, Senegal, and tested the impact of neglecting aerosol non-sphericity on radiative effect calculations. García et al. (2011) did a similar work but at regional level for mixtures of mineral dust and biomass burning and mineral dust and urban/industrial aerosols. García et al. (2012a, b) have used AERONET estimates of the ARF at 40 stations grouped in 14 regions worldwide for six aerosol types: mineral dust, biomass burning, urban/industrial, continental background, oceanic and the free troposphere.

In order to validate AERONET estimations of the solar fluxes we have performed a comparison of the fluxes the most critical for aerosol forcing calculations, namely:

– The solar downward flux at the surface, $F^{\downarrow}_{BOA}$, between AERONET estimations and pyranometer measurements. To perform such a comparison, we have used the Barcelona AERONET/SolRad-Net (Solar Radiation Network, http://solrad-net.gsfc.nasa.gov/) site which is the closest site to our study area in the WMB where collocated AERONET and solar flux measurements are available. The period with

ACPD
doi:10.5194/acp-2015-823

coincident measurements is May 2009–October 2014. The pyranometer is a Kipp and Zonen CMP21 sensor that provides every two minutes a measurement of the total solar flux in the range 0.3–2.8 µm. Coincident AERONET and pyranometer measurement times were restricted to ±1 min. We used SolRad-Net level 1.5 data which have been cleared as free of any operational problems The manufacturer accuracy (2 %) and the sensor drift (< 1 %) yield an overall accuracy on the order of 3 %.

– The solar upward flux at the TOA, $F^{\uparrow}_{\mathrm{TOA}}$, between AERONET estimations and CERES (Clouds and the Earth's Radiant Energy System) measurements at Ersa, Palma and Alborán. We used CERES Single Scanner Footprint (SSF) Level2 products, namely the shortwave (0–5 µm) upward flux at the TOA given for a spatial resolution equivalent to its instantaneous footprint (nadir resolution 20 km equivalent diameter). Measurements from CERES/Aqua and CERES/Terra were used indistinctively. We screened CERES data spatially by accounting only for the pixels in which one of the ground sites falls, and temporally allowing a time difference of ±15 min. The time of overpass of both CERES/Aqua and CERES/Terra over the three sites varies in the range 10–14 UT. The CERES/Terra instantaneous shortwave TOA flux uncertainties is estimated to be 13.5 $\mathrm{W\,m^{-2}}$ for all-sky conditions (https://eosweb.larc.nasa.gov/sites/default/files/project/ceres/quality_summaries/ssf_toa_terra_ed2B.pdf). According to Loeb et al. (2007) CERES/Aqua TOA flux errors are similar. Because of the CERES overpass time (10–14 UT) the SZA restriction for AERONET level 2.0 data ($50 < \mathrm{SZA} < 80^{\circ}$) rejects many measurements that coincide in time but are for $\mathrm{SZA} < 50^{\circ}$. Consequently the use of AERONET level 2.0 data provides very few points for comparison. We have therefore selected AERONET level 1.5 data and checked that now $40 < \mathrm{SZA} < 80^{\circ}$ and that the cases with $40 < \mathrm{SZA} < 50^{\circ}$ represent ∼ 33 % of the total. To further filter CERES data points, we had to deal with two more issues: (1) sometimes CERES pixels are affected by clouds (when at the coincident time AERONET is not), and (2) because the three sites are in

ACPD
doi:10.5194/acp-2015-823

coastline regions CERES pixels contain information from both land and water. The first issue is due to the different techniques used by both AERONET sunphotometers and CERES which make the air mass volumes sampled by both instruments quite different. The second one is in general not problematic, except at given periods of the year and at given hours of the day when the sun glint produces a significant increment of the upward fluxes in the direction of the spaceborne sensor. Both cases result in an increase of CERES upward fluxes at the TOA. To discard those cases, we eliminated from the comparison all pairs of points (CERES, AERONET) that have a difference larger than CERES uncertainty, i.e. 13.5 $W m^{-2}$. The AERONET level 1.5 data are from 2008–2014 in Ersa, 2011–2014 in Palma and 2011–2012 in Alborán.

Figure 10a shows the comparison of downward solar fluxes at the BOA measured by pyranometers vs. estimated by AERONET. A very good agreement is found between both quantities (correlation coefficient, R, greater than 0.99). To quantify the level of accuracy we calculated the average difference between the AERONET modeled and observed flux. We found +12 $W m^{-2}$ which, in relative terms, corresponds to an overestimation of AERONET fluxes of +3.0 %, increment found by dividing the average AERONET modeled flux by the observed one. This value is in the range of mean relative errors (−0.6, +8.5 %) found by García et al. (2008) under different aerosol environments at 9 stations worldwide. Derimian et al. (2008) found an overestimation of approximately +4 % in M'Bour, Senegal. According to García et al. (2008) that overestimation is due mostly to the cosine effect (the pyranometer angular response which can deviate up to ±3 % from the truth at SZA of 70–80°) and the surface albedo and bidirectional reflectance distribution function (BRDF) assumed by AERONET. The least-square fit lineal equation relating the AERONET (AER) fluxes to the observation (OBS) is OBS = 0.98 · AER − 4.50. Our results are in total agreement with García et al. (2008) who found OBS = 0.98 · AER − 5.32. The next step would be to validate the AERONET estimations of ARF against observations. Unfortunately no systematic surface radiative forcing measurements are available in or in the vicinity of Barcelona. However, since

ACPD
doi:10.5194/acp-2015-823

the validation of $F^{\downarrow}_{BOA}$ has been performed regardless of the aerosol load, we can easily assume that the fluxes with turbid (high aerosol load) or clean (low aerosol load) atmospheres follow the same regression line (OBS = 0.98 · AER – 4.50). Finally, to correct for the missing upward fluxes in the definition of ARF^{AER}_{BOA}, the latter can be multiplied by the term (1 – SA) where SA stands for surface albedo. Indeed:

$$\begin{aligned} ARF_{BOA} &= \Delta F^{w}_{BOA} - \Delta F^{o}_{BOA} \\ &= \left(F^{w\downarrow}_{BOA} - F^{w\uparrow}_{BOA}\right) - \left(F^{o\downarrow}_{BOA} - F^{o\uparrow}_{BOA}\right) \\ &= \left(F^{w\downarrow}_{BOA} - SA \cdot F^{w\downarrow}_{BOA}\right) - \left(F^{o\downarrow}_{BOA} - SA \cdot F^{o\downarrow}_{BOA}\right) \\ &= \left(F^{w\downarrow}_{BOA} - F^{o\downarrow}_{BOA}\right)(1 - SA) \end{aligned} \quad (8)$$

Consequently the corrected estimated solar ARF at the BOA, ARF^{c}_{BOA} in $W\,m^{-2}$, has been calculated from the original AERONET radiative forcing, ARF^{AER}_{BOA}, as:

$$ARF^{c}_{BOA} = 0.98 \cdot ARF^{AER}_{BOA} \cdot (1 - SA) \quad (9)$$

The term 0.98 comes from the correction of the fluxes. We have considered a unique value of SA calculated as the average of the surface albedo at the four AERONET wavelengths (440, 675, 870 and 1020 nm). García et al. (2012b) document that considering the surface albedo at the four AERONET wavelengths yields differences less than 10 % w.r.t. considering spectral surface albedo in the whole solar spectral range (0.2–4.0 µm). The corrected solar ARFE at the BOA, $ARFE^{c}_{BOA}$ in $W\,m^{-2}\,AOD^{-1}_{550}$, defined here as the ratio of forcing per unit of AOD at 550 nm, can be simply calculated from the original AERONET ARFE, $ARFE^{AER}_{BOA}$, as:

$$ARFE^{c}_{BOA} = 0.98 \cdot ARFE^{AER}_{BOA} \cdot (1 - SA) \quad (10)$$

Figure 10b shows the comparison of upward solar fluxes at the TOA measured by CERES vs. estimated by AERONET. Here again, but in a lesser extent compared to the

ACPD
doi:10.5194/acp-2015-823

validation of $F^{\downarrow}_{BOA}$, a good agreement is found between both quantities ($R > 0.92$). The average difference between the AERONET modeled and observed flux is $-1.5\,W\,m^{-2}$ which, in relative terms, corresponds to an underestimation of AERONET fluxes of $-1.6\,\%$. To our knowledge it is the first time that AERONET fluxes at the TOA are validated with satellite measurements. The least-square fit lineal equation relating the AERONET (AER) fluxes to the observation (OBS) is OBS = 0.99·AER+2.51. Like at the BOA, since the validation of $F^{\uparrow}_{TOA}$ has been performed regardless of the aerosol load, the correction of the fluxes can be assumed the same for atmospheres with and without aerosols. Then the corrected ARF at the TOA, ARF^{c}_{TOA}, and the corrected ARFE at the TOA, $ARFE^{c}_{TOA}$, write:

$$ARF^{c}_{TOA} = 0.99 \cdot ARF^{AER}_{TOA} \quad (11)$$

$$ARFE^{c}_{TOA} = 0.99 \cdot ARFE^{AER}_{TOA} \quad (12)$$

The monthly means of the corrected AERONET instantaneous solar ARF and ARFE are shown in Fig. 11 at both the BOA and the TOA. By plotting the whole dataset of ARF and ARFE as a function of SZA we have observed that both quantities remained approximately constant independently of SZA. However as SZA increases, the slant path increases and it is logical to expect a decrease of the ARF/ARFE related to the decrease of the solar radiation reaching the Earth. This effect has been observed on instantaneous ARFE observations by Di Sarra et al. (2008) and Di Biagio et al. (2009), among others. We therefore decided to filter Fig. 11 for SZA $\leq 60^{\circ}$.

The solar ARF is strictly negative and shows a marked annual cycle (at both the BOA and the TOA) at both Ersa and Palma. The solar ARF is lower (in absolute value) during the winter months and reaches maxima (in absolute value) in spring or summer. At the BOA, a maximum (in absolute value) of $-20.6\,W\,m^{-2}$ is reached at Ersa in March (with a seasonal maximum of $-18.0\,W\,m^{-2}$ in spring) while the strongest forcing in Palma, $-26.4\,W\,m^{-2}$, is reached in June (with a seasonal maximum of $-22.8\,W\,m^{-2}$ in summer). During the first months of the year (until April) ARF is more than double in

ACPD
doi:10.5194/acp-2015-823

Ersa than in Palma. It reflects a similar result found earlier on AOD^{f}_{440} (see Sect. 4.1 and Fig. 3) and attributed to the contribution of aerosols of continental origin already in spring over Corsica and not before summer over the Balearic Islands. This result is expected since a higher amount of small particles causes more cooling (Tegen and Lacis, 1996). The marked peak in July in Palma (correlated with a peak in AOD_{440}, see Fig. 3a) is clearly due to mineral dust outbreaks which are more frequent in summer. Another effect sums up: in summer $AAOD_{440}$ (Fig. 4) is more than double in Palma (0.043; $SSA_{440} \sim 0.92$) than in Ersa (0.018; $SSA_{440} \sim 0.96$) in summer. According to Boucher and Tanré (2000), the surface forcing is enhanced when the aerosol absorption is larger. At the TOA, the seasonal cycles are similar at both sites. Maxima (in absolute value) are reached during the same month, July, and the same season, summer. The July and summer means are, respectively, -14.5 and $-12.8\,W\,m^{-2}$ in Ersa and -13.9 and $-13.0\,W\,m^{-2}$ in Palma. The same difference observed on ARF_{BOA} during the first months of the year is also visible on ARF_{TOA}: ARF_{TOA} in Ersa is almost double (in absolute value) that in Palma; whereas the stronger influence of the dust outbreaks in Palma (vs. Ersa) on ARF_{BOA} during the summer months is not visible at the TOA. This seems to indicate that ARF_{TOA} is not as much affected by dust long-range transport as it is by long-range transport of small particles of continental origin. As far as aerosol absorption is concerned, Boucher and Tanré (2000) showed that increasing the aerosol absorption decreases the aerosol effect at the TOA. The results in Alborán at both the BOA/TOA in summer ($-27.8/-18.8\,W\,m^{-2}$) and autumn ($-18.3/-13.4\,W\,m^{-2}$) show higher ARF than in the other two sites.

The comparison with the literature is not trivial because of the location of the three sites we chose: clean, insular sites at the crossroads of European and North African air masses; and the limited sun position ($50 < SZA < 60^{\circ}$). Concerning the background aerosols, García et al. (2012a) showed that for oceanic (region R13) and clean (free troposphere, region R14) sites the annual ARF given for $SZA = 60 \pm 5^{\circ}$ was low ($< 10\,W\,m^{-2}$) and rather similar at the BOA and TOA ($ARF_{TOA}/ARF_{BOA} > 0.7$). The situation $ARF_{TOA}/ARF_{BOA} > 0.7$ is found in Ersa in autumn and in Palma in winter

ACPD
doi:10.5194/acp-2015-823

and spring and may indicate the seasons at each site when background aerosols dominate. It is worth further comparing our results to those of García et al. (2012a, b), in particular from the regions R1 (the northern part of the Sahara-Sahel desert area; mineral dust) and R8 (Europe; urban and industrial pollution) which surround our study area. Interestingly in R8 the largest ARF_{BOA} is reached during winter/spring ($-65 < ARF_{BOA} < -45\,W\,m^{-2}$). The same phenomenon occurs in Ersa but with lower values ($ARF_{BOA} \sim -18\,W\,m^{-2}$). A similar ARF summer/autumn cycle (in terms of shape) is also observed between Alborán and R1. The strongest values of ARF_{BOA} (ARF_{TOA}) are reached in summer: around -60 (-20) $W\,m^{-2}$ in R1 and around -28 (-19) $W\,m^{-2}$ in Alborán. We believe that the ratio ARF_{TOA}/ARF_{BOA} is higher in Alborán than in R1 because (1) the dust transport in Alborán occurs at higher altitude and the aerosol vertical distribution produces a significant effect on the fluxes at the TOA (Meloni et al., 2005), and (2) the days dominated by desert dust do not represent more than 31 % of the Alborán data (see Sect. 3.2). Alborán measurements can also be compared to ARF of dust in Granada (140 km N–NW of Alborán) from Valenzuela et al. (2012a) who found annual means of ARF_{BOA} (ARF_{TOA}) at SZA = $55 \pm 5^{\circ}$ of approximately -50 (-20) $W\,m^{-2}$. Here again ARF_{TOA}/ARF_{BOA} is higher in Alborán than in Granada. We believe it is due to low aerosol absorption properties (see Sects. 4.2 and 4.3) in Alborán resulting in relatively large SSA, and therefore in larger ARF_{TOA} (Boucher and Tanré, 2000). Our findings are usually lower than results from case studies: Derimian et al. (2008) found dust ARF_{BOA} (ARF_{TOA}) at SZA = 50° and $AOD_{440} = 0.54$ on the order of -80 (-25) $W\,m^{-2}$ in M'Bour, Senegal; Cachorro et al. (2008) found dust ARF_{BOA} (ARF_{TOA}) at $53 < SZA < 75^{\circ}$ and $AOD_{440} \sim 0.5$ on the order of -60 (-30) $W\,m^{-2}$ in El Arenosillo, Spain; Lyamani et al. (2006) found ARF_{BOA} (ARF_{TOA}) at SZA = 50° of -43 (-8) $W\,m^{-2}$ for dust and -33 (-8) $W\,m^{-2}$ for European–Mediterranean air masses in Granada, Spain; Formenti et al. (2002) found for aged biomass burning with $AOD_{500} = 0.39$ an ARF_{BOA} (ARF_{TOA}) relatively constant with SZA on the order of -78 (-26) $W\,m^{-2}$ in northeastern Greece. In Lampedusa, Italy, under a weak dust intrusion

ACPD
doi:10.5194/acp-2015-823

(AOD_{500} = 0.23 and SSA = 0.96) Meloni et al. (2005) found an ARF_{BOA} (ARF_{TOA}) at SZA = 50° on the order of −13 (−7) W m^{-2}, lower than the summer means at any of the three stations presented in our work. A few years later at the same site but under a strong dust intrusion (AOD_{500} = 0.59) Meloni et al. (2015) found an ARF_{BOA} (ARF_{TOA}) at SZA = 55° on the order of −63 (−45) W m^{-2}, much larger than the summer means found in our work.

The aerosol radiative forcing efficiency in Ersa shows a clear annual cycle, the one at the TOA being reverse of the one at the BOA. Relatively constant minimum absolute values at the BOA [−150; −134 W m^{-2}] are reached during the period April–October while maximum absolute values at the TOA [−107; −100 W m^{-2}] are reached during the same period. The ARFE in Palma also shows a clear annual cycle but with some irregularities compared to Ersa. $ARFE_{BOA}$ reaches minimum absolute values from February to October [−133; −117 W m^{-2}], excepting the month of June, while $ARFE_{TOA}$ has a triangular shape with a maximum in January (−110 W m^{-2}) and a minimum in June (−71 W m^{-2}). The reverse behaviour of $ARFE_{BOA}$ (maximum) and $ARFE_{TOA}$ (minimum) in June is due to the combination of (1) the strong increase (in absolute value) of ARF_{BOA} between May and June while ARF_{TOA} increases very little and (2) the strong increase of AOD from May to June (Fig. 3a). The annual mean of $ARFE_{TOA}$ is lower in Palma (−85.1 W m^{-2}, $SSA_{440} \sim 0.92$) than in Ersa (−99.2 W m^{-2}, $SSA_{440} \sim 0.96$) which reflects that more absorbing aerosols produce a lower absolute $ARFE_{TOA}$ (García et al., 2012b). In Alborán between June and October $ARFE_{BOA}$ varies between −161 and −117 W m^{-2} and $ARFE_{TOA}$ between −105 and −86 W m^{-2}.

García et al. (2012b) produced summer mean values of $ARFE_{BOA}$ ($ARFE_{TOA}$) for SZA = 60 ± 5° in regions R1 (dust) and R8 (urban/industrial) of approximately −150 (−50) and −165 (−70) W m^{-2}, respectively, and winter mean values in R13 (oceanic) of approximately −145 (−100) W m^{-2}. The annual $ARFE_{BOA}$ in Ersa (−144.4 W m^{-2}) and in Palma (−132.2 W m^{-2}) are slightly lower than the values given by García et al. (2012b) but are within the error bars. The explanation is probably that neither

ACPD
doi:10.5194/acp-2015-823

Ersa nor Palma are dominated by any of the aforementioned aerosol types but are rather representative of a mixture of them. García et al. also showed that the mean $ARFE_{BOA}$ in other dust regions (R2, western Africa) could be lower ($-100\,W\,m^{-2}$). The relatively large (in absolute value) annual $ARFE_{TOA}$ in Ersa ($-99.2\,W\,m^{-2}$) and in Palma ($-85.1\,W\,m^{-2}$) compared to the results of García et al. (2012b) indicate that $ARFE_{TOA}$, like ARF_{TOA}, is not strongly affected by long-range transport aerosols. Other works like Derimian et al. (2008) found dust $ARFE_{BOA}$ ($ARFE_{TOA}$, both w.r.t. AOD_{440}) at SZA = 50° on the order of −150 (−45) $W\,m^{-2}$ in M'Bour, Senegal. Di Sarra et al. (2008) made a multi-year statistical study in Lampedusa, Italy, and found $ARFE_{BOA}$ (w.r.t. AOD_{496}) at $50 < SZA < 60°$ on the order of $-155\,W\,m^{-2}$ for dust and $-135\,W\,m^{-2}$ for biomass burning/industrial aerosols. They all showed that while $ARFE_{BOA}$ for dust is hardly dependent on AOD_{λ}, it is highly dependent on AOD_{λ} for biomass burning/industrial aerosols. Likewise, Di Biagio et al. (2009) found also in Lampedusa $ARFE_{BOA}$ (w.r.t. AOD_{496}) at $50 < SZA < 60°$ on the order of $-180\,W\,m^{-2}$ for dust and $-140\,W\,m^{-2}$ for urban/industrial aerosols in Lampedusa, Italy. During a strong dust intrusion in Lampedusa ($AOD_{500} = 0.59$) Meloni et al. (2015) found an $ARFE_{BOA}$ ($ARFE_{TOA}$, both w.r.t. AOD_{500}) at SZA = 55° on the order of −107 (−77) $W\,m^{-2}$, much lower than previous works at the same site (Di Sarra et al., 2008; Di Biagio et al., 2009) and than the summer means found in our work. The reason given by Meloni et al. (2015) is that they used higher SSA values than the ones associated to mineral dust in Lampedusa.

In summary the aerosol radiative forcing at $50 < SZA < 60°$ in the WMB is usually lower than at sites dominated by only one aerosol type (dust or urban/industrial aerosols). During the summer months when dust episodes are more frequent an increase of ARF_{BOA} is observed at all stations along a NE–SW gradient. At the TOA the same increase is observed but without any NE–SW gradient (Ersa and Palma have roughly the same ARF_{TOA}). The radiative forcing efficiency, which unlike the ARF does not depend on the column aerosol amount, does show neither annual cycles with a regular pattern, nor a NE–SW gradient. The explanation comes from the higher de-

ACPD
doi:10.5194/acp-2015-823

pendency of the ARFE to absorption properties which are quite variable over the WMB and do not present a NE–SW gradient (see Sects. 4.2–4.4).

5 Discussion on NE–SW gradients

Before concluding it is worth discussing the NE–SW gradient found (or not) as a function of the type of the aerosol parameters or effects (extensive or intensive). By aerosol effects we mean here the aerosol radiative forcing and radiative forcing efficiency. Intensive parameters are frequently used to perform aerosol classification (Burton et al., 2012) because, unlike extensive parameters, they do not vary with aerosol amount. In order to establish a potential NE–SW gradient, all three stations are needed. For that reason, the discussion that follows is based on the summer means at the three stations, summer being the season with the largest amount of observations available. The last column of Tables 2–4 indicates if the parameter/effect is an extensive or an intensive parameter/effect and if its summer mean presents a NE–SW gradient, i.e. if it is monotonously increasing or decreasing along a NE–SW axis. Among the parameters/effects discussed in the paper, 7 are extensive (AOD, AOD_f, AAOD, C_V^f, C_V^c, ARF_{BOA} and ARF_{TOA}) and 11 are intensive (AE, AAE, Sphericity, r_V^f, r_V^c, RRI, IRI, SSA, g, $ARFE_{BOA}$ and $ARFE_{TOA}$). This list is far from being exhaustive but it may be sufficient to perform a coarse statistics. We find that 3 extensive (AOD, C_V^c and ARF_{BOA}, 43 % of them) and 3 intensive (AE, r_V^c and Sphericity, 27 % of them) parameters/effects do present a NE–SW gradient. We discarded the aerosol radiative forcing at the TOA because the values at Ersa ($-12.8\,W\,m^{-2}$) and Palma ($-13.0\,W\,m^{-2}$) are nearly the same. Figure 12 shows the correlated variations of the extensive and intensive parameters/effects which show a NE–SW gradient. The higher ratio of extensive (42 %) vs. intensive (27 %) properties presenting a NE–SW gradient indicates that the column aerosol amount has a stronger signature over the WMB than intrinsic (intensive) aerosol properties. All three extensive parameters/effects AOD, C_V^c and ARF_{BOA} increase along the NE–SW axis and are clearly related to the higher frequency and in-

ACPD
doi:10.5194/acp-2015-823

tensity of mineral dust episodes during the summer months. The fact that the increase of AOD and ARF_{BOA} with C_V^c occurs approximately in the same proportions (the plots almost overlap, see Fig. 12) indicates that AOD and ARF_{BOA} are closely related over the WMB. The fact that the plots are nearly straight lines indicates a linear geographical gradient which is in agreement with the long-term study of the regional African dust contribution to PM_{10} over the whole Mediterranean Basin made by Pey et al. (2013) and also with the summer means of the dust contribution to satellite-based AOD retrieved by sector over the whole Mediterranean Basin (Barnaba et al., 2004). Similar results are observed for the intensive parameters: r_V^c and Sphericity decrease quasi-linearly with decreasing AE and in the same proportions along the NE–SW axis. The NE–SW gradient of the two intensive parameters AE and Sphericity is here again driven by mineral dust. In turn, and as explained in Sect. 4.3, the decrease of r_V^c along the NE–SW axis reflects the decreasing influence of European pollution (urban/industrial aerosols median radii are larger than those of dust). This result put together with the increasing C_V^c along the NE–SW axis suggests that the concentration of large particles is higher but their size smaller in relative terms in the southern WMB.

Finally it is worth coming back to the conclusions drawn so far in Sects. 4.1–4.4 about the fine mode of the particle size distribution and the absorption properties. As can be seen in the last column of Tables 2–4, none of the extensive or intensive parameters related to those two aspects present a NE–SW gradient. The absence of NE–SW gradient of r_V^f and C_V^f is due to a homogeneous spatial distribution of the fine particle loads over the three sites in spite of the distances between the sites and the differences in local sources (see Sect. 4.1). The absence of NE–SW gradient of the absorption properties (AAOD, AAE, IRI, SSA) is essentially due to the low values and the absence of spectral dependency of the absorption found in Albóran. These findings raise the questions of the composition and its origin of the aerosol type that seems to drive the absorbing spectral behaviour in Albóran, which apparently is not that of mineral dust only.

ACPD
doi:10.5194/acp-2015-823

6 Conclusions

Four years (2011–2014) of AERONET products are compared in two regional background insular sites in the western Mediterranean Basin, in Corsica and in the Balearic Islands. A few months of AERONET measurements available in a third site in Alborán Island are considered for completing the dataset. All three sites are situated along a NE–SW axis in the WMB.

In Ersa and Palma, products such as AOD, AOD^f, the particle size distribution, the sphericity, the radiative forcing and the radiative forcing efficiency show a clear annual cycle:

- AOD, AOD^f, the fine and coarse mode volume concentrations reach maxima during summertime and minima during wintertime. The shape of the annual cycles is different between both sites because of the inter-season changes. The higher values of AOD and C_V^c in Palma in summer are due to the mineral dust outbreaks which are more frequent in summer and whose frequency and intensity increases along the NE–SW axis. The higher values of AOD, AOD^f and C_V^f in Ersa in spring are due to the contribution of aerosols of continental origin already in spring over Corsica and not before summer over the Balearic Islands.

- The sphericity exhibits minima in summer which are clearly due to the higher frequency of mineral dust outbreaks during this season.

- The radiative forcing at the surface filtered for $50 \leq SZA \leq 60^\circ$ reaches its maximum (in absolute value) during spring ($-18.0\,W\,m^{-2}$) and summer ($-22.8\,W\,m^{-2}$) in Ersa and Palma, respectively. In spring ARF_{BOA} is almost double in Ersa than in Palma. Interestingly, AOD and ARF_{BOA} annual cycles are very well correlated and thus the same reasons explain the differences between the shapes of the ARF_{BOA} annual cycles at both sites. ARF_{TOA} reaches summer maxima (in absolute value) similar at both sites ($\sim -13.0\,W\,m^{-2}$) and values in spring 1.6 times larger in Ersa than in Palma. This result indicates that ARF_{TOA} is not as much affected by dust

ACPD
doi:10.5194/acp-2015-823

long-range transport as it is by long-range transport of small particles of continental origin.

– The radiative forcing efficiency annual cycles show some irregularities and have quite different shapes at both sites. $ARFE_{BOA}$ reaches minimum absolute values during the period April – October in the range [−150; −117 W m^{-2}], while $ARFE_{TOA}$ varies in the range [−107; −71 W m^{-2}] during the same period.

Among the 18 aerosol parameters/effects discussed in the paper, 3 extensive (AOD, C_V^c and ARF_{BOA}) and 3 intensive (AE, r_V^c and Sphericity) parameters present a NE–SW gradient of their summer means. The relationships between (AOD, ARF_{BOA}) vs. C_V^c and (r_V^c, Sphericity) vs. AE are quasi-linear relationships. While the NE–SW gradient of AOD, C_V^c, ARF_{BOA}, AE and Sphericity are clearly related to the higher frequency and intensity of mineral dust episodes during the summer months, the gradient of r_V^c (a decrease along the NE–SW axis) reflects the decreasing influence of European pollution along the NE–SW axis.

Two main conclusions of our work explain why two thirds of the parameters/effects discussed in the paper do not present a NE–SW gradient. First, we have observed a homogeneous spatial distribution (except during the month of March and April) of the fine particle loads over the three sites in spite of the distances between the sites and the differences in local sources. Second, surprisingly low values and the absence of spectral dependency of the absorption were found in Albóran. This finding points out towards the presence of BC and/or soot (possibly originated from North African urban/industrial areas and/or from both the harbor of Algeciras and vessel traffic near the Strait of Gibraltar) and supports the hypothesis of an anthropogenic influenced mineral dust (all 15 summer cases in Alborán correspond to dust events). This hypothesis, already formulated in previous works (Müller et al., 2009; Valenzuela et al., 2015), together with the fact that the absorption is higher and wavelength-dependent at the other two sites, rises an important question for future works: what are the processes which inhibits the BC and/or soot absorption properties during the transport to the northern

ACPD
doi:10.5194/acp-2015-823

part of the WMB? In the framework of ChArMEx, ongoing investigations might bring some light to this subject in the near future.

Acknowledgement. This study is performed in the framework of work package 4 on aerosol-radiation-climate interactions of the coordinated program ChArMEx (the Chemistry-Aerosol Mediterranean Experiment; http://charmex.lsce.ipsl.fr). It is also supported by the ACTRIS (Aerosols, Clouds, and Trace Gases Research Infrastructure Network) Research Infrastructure Project funded by the European Union's Horizon 2020 research and innovation programme under grant agreement n. 654169 and previously under grant agreement n. 262254 in the 7th Framework Programme (FP7/2007-2013); by the Spanish Ministry of Economy and Competitivity (project TEC2012-34575) and of Science and Innovation (project UNPC10-4E-442) and EFRD (European Fund for Regional Development); by the Department of Economy and Knowledge of the Catalan autonomous government (grant 2014 SGR 583); and by the Andalusia Regional Government through projects P12-RNM-2409 and P10-RNM-6299. ChArMEx-France is supported through the MISTRALS program by INSU, ADEME, Météo-France, CEA. The The Spanish Agencia Estatal de Meteorología (AEMET) is acknowledged for the use of the Palma de Mallorca AERONET sun-photometer data, and the Royal Institute and Observatory of the Spanish Navy (ROA) for the support provided in Alborán.

References

Alados-Arboledas, L., Alcántara, A., Olmo, F. J., Martínez-Lozano, J. A., Estellés, V., Cachorro, V., Silva, A. M., Horvath, H., Gangl, M., Díaz, A., Pujadas, M., Lorente, J., Labajo, A., Sorribas, M., and Paves, G.: Aerosol columnar properties retrieved from CIMEL radiometers during VELETA 2002, Atmos. Environ., 42, 2654–2667, 2008.

Albrecht, B. A.: Aerosols, cloud microphysics and fractional cloudiness, Science, 245, 1227–1230, doi:10.1126/science.245.4923.1227, 1989.

Barnaba, F. and Gobbi, G. P.: Aerosol seasonal variability over the Mediterranean region and relative impact of maritime, continental and Saharan dust particles over the basin from MODIS data in the year 2001, Atmos. Chem. Phys., 4, 2367–2391, doi:10.5194/acp-4-2367-2004, 2004.

ACPD

doi:10.5194/acp-2015-823

Bergametti, G., Remoudaki, E., Losno, R., Steiner, E., Chatenet, B., and Buat-Mnard, P.: Source, transport and deposition of atmospheric phosphorus over the northwestern Mediterranean, J. Atmos. Chem., 14, 501–513, 1992.

Bergstrom, R. W., Pilewskie, P., Russell, P. B., Redemann, J., Bond, T. C., Quinn, P. K., and Sierau, B.: Spectral absorption properties of atmospheric aerosols, Atmos. Chem. Phys., 7, 5937–5943, doi:10.5194/acp-7-5937-2007, 2007.

Boucher, O. and Tanré, D.: Estimation of the aerosol perturbation to the Earth's radiative budget over oceans using POLDER satellite aerosol retrievals, Geophys. Res. Lett., 27, 1103–1106, 2000.

Burton, S. P., Ferrare, R. A., Hostetler, C. A., Hair, J. W., Rogers, R. R., Obland, M. D., Butler, C. F., Cook, A. L., Harper, D. B., and Froyd, K. D.: Aerosol classification using airborne High Spectral Resolution Lidar measurements – methodology and examples, Atmos. Meas. Tech., 5, 73–98, doi:10.5194/amt-5-73-2012, 2012.

Cachorro, V. E., Toledano, C., Prats, N., Sorribas, M., Mogo, S., Berjón, A., Torres, B., Rodrigo, R., de la Rosa, J., and De Frutos, A. M.: The strongest desert dust intrusion mixed with smoke over the Iberian Peninsula registered with Sun photometry, J. Geophys. Res., 113, D14S04, doi:10.1029/2007JD009582, 2008.

Chazette, P., Marnas, F., and Totems, J.: The mobile Water vapor Aerosol Raman LIdar and its implication in the framework of the HyMeX and ChArMEx programs: application to a dust transport process, Atmos. Meas. Tech., 7, 1629–1647, doi:10.5194/amt-7-1629-2014, 2014.

Denjean, C., Cassola, F., Mazzino, A., Triquet, S., Chevaillier, S., Grand, N., Bourrianne, T., Momboisse, G., Sellegri, K., Schwarzenbock, A., Freney, E., Mallet, M., and Formenti, P.: Size distribution and optical properties of mineral dust aerosols transported in the western Mediterranean, Atmos. Chem. Phys. Discuss., 15, 21607–21669, doi:10.5194/acpd-15-21607-2015, 2015.

Derimian, Y., Léon, J.-F., Dubovik, O., Chiapello, I., Tanré, D., Sinyuk, A., Auriol, F., Podvin, T., Brogniez, G., and Holben, B. N.: Radiative properties of aerosol mixture observed during the dry season 2006 over M'Bour, Senegal (African Monsoon Multidisciplinary Analysis campaign), J. Geophys. Res., 113, D00C09, doi:10.1029/2008JD009904, 2008.

Di Biagio, C., Di Sarra, A., Meloni, D., Monteleone, F., Piacentino, S., and Sferlazzo, D.: Measurements of Mediterranean aerosol radiative forcing and influence of the single scattering albedo, J. Geophys. Res., 114, D06211, doi:10.1029/2008JD011037, 2009.

ACPD

doi:10.5194/acp-2015-823

Di Sarra, A., Pace, G., Meloni, D., De Silvestri, L., Piacentino, S., and Monteleone, F.: Surface shortwave radiative forcing of different aerosol types in the Mediterranean, Geophys. Res. Lett., 35, L02714, doi:10.1029/2007GL032395, 2008.

Dubovik, O. and King, M. D.: A flexible inversion algorithm for retrieval of aerosol optical properties from Sun and sky radiance measurements, J. Geophys. Res., 105, 20673–20696, 2000.

Dubovik, O., Smirnov, A., Holben, B. N., King, M. D., Kaufman, Y. J., Eck, T. F., and Slutsker, I.: Accuracy assessment of aerosol optical properties retrieval from AERONET sun and sky radiance measurements, J. Geophys. Res., 105, 9791–9806, 2000.

Dubovik, O., Holben, B. N., Lapyonok, T., Sinyuk, A., Mishchenko, M. I., Yang, P., and Slutsker, I.: Non-spherical aerosol retrieval method employing light scattering by spheroids, Geophys. Res. Lett., 10, 1415, doi:10.1029/2001GL014506, 2002a.

Dubovik, O., Holben, B. N., Eck, T. F., Smirnov, A., Kaufman, Y. J., King, M. D., Tanré, D., and Slutsker, I.: Variability of absorption and optical properties of key aerosol types observed in worldwide locations, J. Atmos. Sci., 59, 590–608, 2002b.

Dubovik, O., Sinyuk, A., Lapyonok, T., Holben, B. N., Mishchenko, M., Yang, P., Eck, T. F., Volten, H., Muñoz, O., Veihelmann, B., van der Zande, W. J., Leon, J.-F., Sorokin, M., and Slutsker, I.: Application of spheroid models to account for aerosol particle nonsphericity in remote sensing of desert dust, J. Geophys. Res., 111, D11208, doi:10.1029/2005JD006619, 2006.

Dubuisson, P., Buriez, J. C., and Fouquart, Y.: High Spectral resolution solar radiative transfer in absorbing and scattering media, application to the satellite simulation, J. Quant. Spectrosc. Ra., 55, 103–126, 1996.

Dubuisson, P., Dessailly, D., Vesperini, M., and Frouin, R.: Water vapor retrieval over ocean using near-infrared radiometry, J. Geophys. Res., 109, D19106, doi:10.1029/2004JD004516, 2004.

Dubuisson, P., Roger, J., Mallet, M., and Dubovik, O.: A code to compute the direct solar radiative forcing: application to anthropogenic aerosols during the escompte experiment, in: Proc. International Radiation Symposium (IRS 2004) on Current Problems in Atmospheric Radiation, edited by: Fischer, H., Sohn, B.-J., and Deepak, A., Hampton, 23–28 August 2004, Busan, Korea, 127–130, 2006.

ACPD

doi:10.5194/acp-2015-823

Dulac, F.: An overview of the Chemistry-Aerosol Mediterranean Experiment (ChArMEx), European Geosciences Union General Assembly, Geophysical Research Abstracts Vol. 16, EGU2014-11441, 27 April–2 May 2014, Vienna, Austria, 2014.

Eck, T. F., Holben, B. N., Reid, J. S., Dubovik, O. Kinne, S., Smirnov, A., O'Neill, N. T., and Slutsker, I.: The wavelength dependence of the optical depth of biomass burning, urban and desert dust aerosols, J. Geophys. Res., 104, 31333–31349, 1999.

Escudero, M., Querol, X., Ávila, A., and Cuevas, E.: Origin of the exceedances of the European daily PM limit value in regional background areas of Spain, Atmos. Environ., 41, 730–744, 2007.

Formenti, P., Boucher, O. Reiner, T., Sprung, D., Andreae, M. O., Wendisch, M., Wex, H., Kindred, D., Tzortziou, M., Vasaras, A., and Zerefos, C.: STAAARTE-MED 1998 summer airborne measurements over the Aegean Sea: 2. Aerosol scattering and absorption, and radiative calculations, J. Geophys. Res., 107, 4551, doi:10.1029/2001JD001536, 2002.

Freudenthaler, V., Esselborn, M., Wiegner, M., Heese, B., Tesche, M., Ansmann, A., Müller, D., Althausen, D., Wirth, M., Fix, A., Ehret, G., Knippertz, P., Toledano, C., Gasteiger, J., Garhammer, M., and Seefeldner, M.: Depolarization ratio profiling at several wavelengths in pure Saharan dust during SAMUM 2006, Tellus B, 61, 165–179, 2008.

Gangoiti, G., Millán, M. M., Salvador, R., and Mantilla, E.: Long-range transport and recirculation of pollutants in the western Mediterranean during the project Regional Cycles of Air Pollution in the West-Central Mediterranean Area, Atmos. Environ., 35, 6267–6276, 2001.

García, O. E., Díaz, A. M., Expósito, F. J., Díaz, J. P., Dubovik, O., Dubuisson, P., Roger, J.-C., Eck, T. F., Sinyuk, A., Derimian, Y., Dutton, E. G., Schafer, J. S., Holben, B. N., and García, C. A.: Validation of AERONET estimates of atmospheric solar fluxes and aerosol radiative forcing by ground-based broadband measurements, J. Geophys. Res., 113, D21207, doi:10.1029/2008JD010211, 2008.

García, O. E., Expósito, F. J., Díaz, J. P., and Díaz, A. M.: Radiative forcing under aerosol mixed conditions, J. Geophys. Res., 116, D01201, doi:10.1029/2009JD013625, 2011.

García, O. E., Díaz, J. P., Expósito, F. J., Díaz, A. M., Dubovik, O., and Derimian, Y.: Aerosol Radiative Forcing: AERONET-Based Estimates, Climate Models, InTech, available at: http://www.intechopen.com/books/climate-models/aerosol-radiative-forcing-aeronet-based-estimates (last access: 16 December 2015), 2012a.

ACPD
doi:10.5194/acp-2015-823

García, O. E., Díaz, J. P., Expósito, F. J., Díaz, A. M., Dubovik, O., Derimian, Y., Dubuisson, P., and Roger, J.-C.: Shortwave radiative forcing and efficiency of key aerosol types using AERONET data, Atmos. Chem. Phys., 12, 5129–5145, doi:10.5194/acp-12-5129-2012, 2012b.
Giorgi, F.: Climate change hot-spots, Geophys. Res. Lett., 33, L08707, doi:10.1029/2006GL025734, 2006.
Giorgi, F. and Lionello, P.: Climate change projections for the Mediterranean region, Global Planet. Change, 63, 90–104, 2008.
Gkikas, A., Houssos, E. E., Hatzianastassiou, N., Papadimas, C. D., and Bartzokas, A.: Synoptic conditions favouring the occurrence of aerosol episodes over the broader Mediterranean basin, Q. J. Roy. Meteor. Soc., 138, 932–949, doi:10.1002/qj.978, 2012.
Holben, B. N., Eck, T. F., Slutsker, I., Tanré, D., Buis, J. P., Setzer, A., Vermote, E. F., Reagan, J. A., Kaufman, Y. J., Nakajima, T., Lavenu, F., Jankowiak, I., and Smirnov, A.: AERONET – a federated instrument network and data archive for aerosol characterization, Remote Sens. Environ., 66, 1–16, 1998.
Holben, B. N., Eck, T. F., Slutsker, I., Smirnov, A., Sinyuk, A., Schafer, J., Giles, D., and Dubovik, O.: AERONET's Version 2.0 quality assurance criteria, in: Remote Sensing of the Atmosphere and Clouds, edited by: Tsay, S.-C., Nakajima, T., Ramesh, P. S., and Sridharan, R., Proc. of SPIE, 6408, 64080Q, doi:10.1117/12.706524, 2006.
Hurrell, J. W.: Decadal trends in the North Atlantic Oscillation: regional temperatures and precipitation, Science, 269, 676–679, 1995.
Kallos, G., Cortón, V., Lagouvardos, K., and Papadopoulos, A.: On the long range transport of air pollutants from Europe to Africa, Geophys. Res. Lett., 25, 619–622, 1998.
Kallos, G., Astitha, M., Katsafados, P., and Spyrou, C.: Long-range transport of anthropogenically and naturally produced particulatematter in the Mediterranean and North Atlantic: current state of knowledge, J. Appl. Meteorol. Clim., 46, 1230–1251, 2007.
Lack, D. A. and Cappa, C. D.: Impact of brown and clear carbon on light absorption enhancement, single scatter albedo and absorption wavelength dependence of black carbon, Atmos. Chem. Phys., 10, 4207–4220, doi:10.5194/acp-10-4207-2010, 2010.
Lambert, D. and Argence, S.: Preliminary study of an intense rainfall episode in Corsica, 14 September 2006, Adv. Geosci., 16, 125–129, doi:10.5194/adgeo-16-125-2008, 2008.
Lambert, D., Mallet, M., Ducrocq, V., Dulac, F., Gheusi, F., and Kalthoff, N.: CORSiCA: a Mediterranean atmospheric and oceanographic observatory in Corsica within the frame-

ACPD
doi:10.5194/acp-2015-823

work of HyMeX and ChArMEx, Adv. Geosci., 26, 125–131, doi:10.5194/adgeo-26-125-2011, 2011.

Lelieveld, J., Berresheim, H., Borrmann, S., Crutzen, P. J., Dentener, F. J., Fischer, H., Feichter, J., Flatau, P. J., Heland, J., Holzinger, R., Korrmann, R., Lawrence, M. G., Levin, Z., Markowicz, K. M., Mihalopoulos, N., Minikin, A., Ramanathan, V., de Reus, M., Roelofs, G. J., Scheeren, H. A., Sciare, J., Schlager, H., Schultz, M., Siegmund, P., Steil, B., Stephanou, E. G., Stier, P., Traub, M., Warneke, C., Williams, J., and Ziereis, H.: Global air pollution crossroads over the Mediterranean, Science, 298, 794–799, 2002.

Léon, J.-F., Augustin, P., Mallet, M., Bourrianne, T., Pont, V., Dulac, F., Fourmentin, M., Lambert, D., and Sauvage, B.: Aerosol vertical distribution, optical properties and transport over Corsica (western Mediterranean), Atmos. Chem. Phys. Discuss., 15, 9507–9540, doi:10.5194/acpd-15-9507-2015, 2015.

Loeb, N. G., Kato, S., Loukachine, K., Manalo-Smith, N., and Doelling, D. R.: Angular distribution models for top-of-atmosphere radiative flux estimation from the clouds and the earth's radiant energy system instrument on the terra satellite – Part II: validation, J. Atmos. Ocean. Tech., 24, 564–584, doi:10.1175/JTECH1983.1, 2007.

Lurton, T., Renard, J.-B., Vignelles, D., Jeannot, M., Akiki, R., Mineau, J.-L., and Tonnelier, T.: Light scattering at small angles by atmospheric irregular particles: modelling and laboratory measurements, Atmos. Meas. Tech., 7, 931–939, doi:10.5194/amt-7-931-2014, 2014.

Lyamani, H., Olmo, F. J., Alcántara, A., and Alados-Arboledas, L.: Atmospheric aerosols during the 2003 heat wave in southeastern Spain II: microphysical columnar properties and radiative forcing, Atmos. Environ., 40, 6465–6476, 2006.

Lyamani, H., Valenzuela, A., Perez-Ramirez, D., Toledano, C., Granados-Muñoz, M. J., Olmo, F. J., and Alados-Arboledas, L.: Aerosol properties over the western Mediterranean basin: temporal and spatial variability, Atmos. Chem. Phys., 15, 2473–2486, doi:10.5194/acp-15-2473-2015, 2015.

Maheras, P., Xoplaki, E., Davies, T., Vide, J. V., Bariendos, M., and Alcoforado, M.: Warm and cold monthly anomalies across the Mediterranean basin and their relationship with circulation: 1860–1990, Int. J. Climatol., 19, 1697–1715, 1999.

Mallet, M., Dubovik, O., Nabat, P., Dulac, F., Kahn, R., Sciare, J., Paronis, D., and Léon, J. F.: Absorption properties of Mediterranean aerosols obtained from multi-year ground-based remote sensing observations, Atmos. Chem. Phys., 13, 9195–9210, doi:10.5194/acp-13-9195-2013, 2013.

ACPD
doi:10.5194/acp-2015-823

Mallet, M., Dulac, F., Formenti, P., Nabat, P., Sciare, J., Roberts, G., Pelon, J., Ancellet, G., Tanré, D., Parol, F., di Sarra, A., Alados, L., Arndt, J., Auriol, F., Blarel, L., Bourrianne, T., Brogniez, G., Chazette, P., Chevaillier, S., Claeys, M., D'Anna, B., Denjean, C., Derimian, Y., Desboeufs, K., Di Iorio, T., Doussin, J.-F., Durand, P., Féron, A., Freney, E., Gaimoz, C., Goloub, P., Gómez-Amo, J. L., Granados-Muñoz, M. J., Grand, N., Hamonou, E., Jankowiak, I., Jeannot, M., Léon, J.-F., Maillé, M., Mailler, S., Meloni, D., Menut, L., Momboisse, G., Nicolas, J., Podvin, J., Pont, V., Rea, G., Renard, J.-B., Roblou, L., Schepanski, K., Schwarzenboeck, A., Sellegri, K., Sicard, M., Solmon, F., Somot, S., Torres, B., Totems, J., Triquet, S., Verdier, N., Verwaerde, C., Wenger, J., and Zapf, P.: Overview of the Chemistry-Aerosol Mediterranean Experiment/Aerosol Direct Radiative Forcing on the Mediterranean Climate (ChArMEx/ADRIMED) summer 2013 campaign, Atmos. Chem. Phys. Discuss., 15, 19615–19727, doi:10.5194/acpd-15-19615-2015, 2015.

Mariotti, A., Pan, Y., Zeng, N., and Alessandri, A.: Long-term climate change in the Mediterranean region in the midst of decadal variability, Clim. Dynam., 44, 1437–1456, doi:10.1007/s00382-015-2487-3, 2015.

Markowicz, K. M., Flatau, P. J., Ramana, M. V., Crutzen, P. J., and Ramanathan, V.: Absorbing mediterranean aerosols lead to a large reduction in the solar radiation at the surface, Geophys. Res. Lett., 29, 1968, doi:10.1029/2002GL015767, 2002.

Meloni, D., di Sarra, A., Di Iorio, T., and Fiocco, G.: Influence of the vertical profile of Saharan dust on the visible direct radiative forcing, J. Quant. Spectrosc. Ra., 93, 397–413, 2005.

Meloni, D., Junkermann, W., di Sarra, A., Cacciani, M., De Silvestri, L., Di Iorio, T., Estellés, V., Gómez-Amo IV, J. L., Pace, G., and Sferlazzo, D. M.: Altitude-resolved shortwave and longwave radiative effects of desert dust in the Mediterranean during the GAMARF campaign: indications of a net daily cooling in the dust layer, J. Geophys. Res., 120, 3386–3407, doi:10.1002/2014JD022312, 2015.

Millán, M. M., Salvador, R., Mantilla, E., and Kallos, G.: Photooxidant dynamics in the Mediterranean basin in summer: results from European research projects, J. Geophys. Res., 102, 8811–8823, 1997.

Mishra, A. K., Klingmueller, K., Fredj, E., Lelieveld, J., Rudich, Y., and Koren, I.: Radiative signature of absorbing aerosol over the eastern Mediterranean basin, Atmos. Chem. Phys., 14, 7213–7231, doi:10.5194/acp-14-7213-2014, 2014.

Moosmüller, H., Chakrabarty, R. K., and Arnott, W. P.: Aerosol light absorption and its measurement: a review, J. Quant. Spectrosc. Ra., 110, 844–878, 2009.

ACPD
doi:10.5194/acp-2015-823

Moulin, C., Lambert, C. E., Dayan, U., Masson, V., Ramonet, M., Bousquet, P., Legrand, M., Balkanski, Y. J., Guelle, W., Marticorena, B., Bergametti, G., and Dulac, F.: Satellite climatology of African dust transport in the Mediterranean atmosphere, J. Geophys. Res., 103, 13137–13144, 1998.

Müller, T., Schladitzm, A., Massling, A., Kaaden, N., Kandler, K., and Wiedensohler, A.: Spectral absorption coefficients and imaginary parts of refractive indices of Saharan dust during SAMUM-1, Tellus B, 61, 79–95, 2009.

Nabat, P., Solmon, F., Mallet, M., Kok, J. F., and Somot, S.: Dust emission size distribution impact on aerosol budget and radiative forcing over the Mediterranean region: a regional climate model approach, Atmos. Chem. Phys., 12, 10545–10567, doi:10.5194/acp-12-10545-2012, 2012.

Nabat, P., Somot, S., Mallet, M., Chiapello, I., Morcrette, J. J., Solmon, F., Szopa, S., Dulac, F., Collins, W., Ghan, S., Horowitz, L. W., Lamarque, J. F., Lee, Y. H., Naik, V., Nagashima, T., Shindell, D., and Skeie, R.: A 4-D climatology (1979–2009) of the monthly tropospheric aerosol optical depth distribution over the Mediterranean region from a comparative evaluation and blending of remote sensing and model products, Atmos. Meas. Tech., 6, 1287–1314, doi:10.5194/amt-6-1287-2013, 2013.

Nakajima, T., Tonna, G., Rao, R., Boi, P., Kaufman, Y., and Holben, B.: Use of sky brightness measurements from ground for remote sensing of particulate dispersion, Appl. Optics, 35, 2672–2686, 1996.

Norris, J. R. and Wild, M.: Trends in aerosol radiative effects over Europe inferred from observed cloud cover, solar "dimming" and solar "brightening", J. Geophys. Res., 112, D08214, doi:10.1029/2006JD007794, 2007.

Olmo, F. J., Quirantes, A., Lara, V., Lyamani, H., and Alados-Arboledas, L.: Aerosol optical properties assessed by an inversion method using the solar principal plane for non-spherical particles, J. Quant. Spectrosc. Ra., 109, 1504–1516, 2008.

Omar, A. H., Won, J. G., Winker, D. M., Yoon, S. C., Dubovik, O., and McCormick, M. P.: Development of global aerosol models using cluster analysis of Aerosol Robotic Network (AERONET) measurements, J. Geophys. Res., 110, D10S14, doi:10.1029/2004JD004874, 2005.

O'Neill, N. T., Dubovik, O., and Eck, T. F.: A modified Angstrom coefficient for the characterization of sub-micron aerosols, Appl. Optimizat., 40, 2368–2374, 2001.

ACPD

doi:10.5194/acp-2015-823

O'Neill, N. T., Eck, T. F., Smirnov, A., Holben, B. N., and Thulasiraman, S.: Spectral discrimination of coarse and fine mode optical depth, J. Geophys. Res., 108, 4559–4573, doi:10.1029/2002JD002975, 2003.

Pandolfi, M., Gonzalez-Castanedo, Y., Alastuey, A., de la Rosa, J. D., Mantilla, E., Sanchez de la Campa, A., Querol, X., Pey, J., Amato, F., and Moreno, T.: Source apportionment of PM_{10} and $PM_{2.5}$ at multiple sites in the strait of Gibraltar by PMF: impact of shipping emissions, Environ. Sci. Pollut. R., 18, 260–269, doi:10.1007/s11356-010-0373-4, 2011.

Papadimas, C. D., Hatzianastassiou, N., Mihalopoulos, N., Querol, X., and Vardavas, I.: Spatial and temporal variability in aerosol properties over the Mediterranean basin based on 6 year (2000–2006) MODIS data, J. Geophys. Res., 113, D11205, doi:10.1029/2007JD009189, 2008.

Pérez, C., Sicard, M., Jorba, O., Comerón, A., and Baldasano, J. M.: Summertime recirculations of air pollutants over the North-Eastern Iberian coast observed from systematic earlinet lidar measurements in Barcelona, Atmos. Environ., 38, 3983–4000, 2004.

Petzold, A., Rasp, K., Weinzierl, B., Esselborn, M., Hamburger, T., Dörnbrack, A., Kandler, K., Schütz, L., Knippertz, P., Fiebig, M., and Virkkula, A.: Saharan dust absorption and refractive index from aircraft-based observations during SAMUM 2006, Tellus B, 61, 118–130, 2009.

Pey, F., Querol, X., and Alastuey, A.: Variations of levels and composition of PM_{10} and $PM_{2.5}$ at an insular site in the Western Mediterranean, Atmos. Res., 94, 285–299, 2009.

Pey, J., Querol, X., Alastuey, A., Forastiere, F., and Stafoggia, M.: African dust outbreaks over the Mediterranean Basin during 2001–2011: PM_{10} concentrations, phenomenology and trends, and its relation with synoptic and mesoscale meteorology, Atmos. Chem. Phys., 13, 1395–1410, doi:10.5194/acp-13-1395-2013, 2013.

Pincus, R. and Baker, M. B.:Precipitation, solar absorption, and albedo susceptibility in marine boundary layer clouds, Nature, 372, 250–252, doi:10.1038/372250a0, 1994.

Pruppacher, H. R. and Klett, J. D.: Microphysics of Clouds and Precipitation, Kluwer Academic Publishers, Dordrecht, the Netherlands, 1997.

Redemann, J., Turco, R. P., Liou, K. N., Russell, P. B., Bergstrom, R. W., Schmid, B., Livingston, J. M., Hobbs, P. V., Hartley, W. S., Ismail, S., Ferrare, R. A., and Browell, E. V.: Retrieving the vertical structure of the effective aerosol complex index of refraction from a combination of aerosol in situ and remote sensing measurements during TARFOX, J. Geophys. Res., 105, 9949–9970, 2000.

ACPD
doi:10.5194/acp-2015-823

Renard, J.-B., Dulac, F., Berthet, G., Lurton, T., Vignelles, D., Jégou, F., Tonnelier, T., Thaury, C., Jeannot, M., Couté, B., Akiki, R., Mineau, J.-L., Verdier, N., Mallet, M., Gensdarmes, F., Charpentier, P., Mesmin, S., Duverger, V., Dupont, J.-C., Elias, T., Crenn, V., Sciare, J., Giacomoni, J., Gobbi, M., Hamonou, E., Olafsson, H., Dagsson-Waldhauserova, P., Camy-Peyret, C., Mazel, C., Décamps, T., Piringer, M., Surcin, J., and Daugeron, D.: LOAC: a small aerosol optical counter/sizer for ground-based and balloon measurements of the size distribution and nature of atmospheric particles – Part 1: Principle of measurements and instrument evaluation, Atmos. Meas. Tech. Discuss., 8, 1203–1259, doi:10.5194/amtd-8-1203-2015, 2015.

Rodríguez, S., Alastuey, A., Alonso-Pérez, S., Querol, X., Cuevas, E., Abreu-Afonso, J., Viana, M., Pérez, N., Pandolfi, M., and de la Rosa, J.: Transport of desert dust mixed with North African industrial pollutants in the subtropical Saharan Air Layer, Atmos. Chem. Phys., 11, 6663–6685, doi:10.5194/acp-11-6663-2011, 2011.

Russell, P. B., Bergstrom, R. W., Shinozuka, Y., Clarke, A. D., DeCarlo, P. F., Jimenez, J. L., Livingston, J. M., Redemann, J., Dubovik, O., and Strawa, A.: Absorption Angstrom Exponent in AERONET and related data as an indicator of aerosol composition, Atmos. Chem. Phys., 10, 1155–1169, doi:10.5194/acp-10-1155-2010, 2010.

Sanchez-Gomez, E., Somot, S., and Mariotti, A.: Future changes in the Mediterranean water budget projected by an ensemble of regional climate models, Geophys. Res. Lett., 36, L21401, doi:10.1029/2009GL040120, 2009.

Sciare, J., Dulac, F., Feron, A., Crenn, V., Sarda Esteve, R., Baisnee, D., Bonnaire, N., Hamonou, E., Mallet, M., Lambert, D., Nicolas, J. B., Bourrianne, T., Petit, J. E., Favez, O., Canonaco, F., Prevot, A., Mocnik, G., Drinovec, L., Marpillat, A., and Serrie, W.: Carbonaceous aerosols in the Western Mediterranean during summertime and their contribution to the aerosol optical properties at ground level: first results of the ChArMEx-ADRIMED 2013 intensive campaign in Corsica, European Geosciences Union General Assembly, Geophysical Research Abstracts, Vol. 16, EGU2014-2358, 27 April–2 May 2014, Vienna, Austria, 2014.

Sicard, M., Pérez, C., Rocadenbosch, F., Baldasano, J. M., and García-Vizcaino, D.: Mixed-layer depth determination in the Barcelona coastal area from regular lidar measurements: methods, results and limitations, Bound.-Lay. Meteorol., 119, 135–157, 2006.

Sicard, M., Totems, J., Barragan, R., Dulac, F., Mallet, M., Comerón, A., Alados-Arboledas, L., Augustin, P., Chazette, P., Léon, J.-F., Olmo, F. J., Renard, J.-B., and Rocadenbosch, F.:

ACPD
doi:10.5194/acp-2015-823

Variability of Mediterranean aerosols properties at three regional background sites in the western Mediterranean Basin, in: Proc. SPIE 9242, edited by: Comerón, A., Kassianov, E. I., Schäfer, K., Picard, R. H., Stein, K., and Gonglewski, J. D., SPIE, Washington (EE.UU.), USA, CCC code: 0277-786X/14/$18, doi:10.1117/12.2068694, 2014.

Sinyuk, A., Dubovik, O., Holben, B. N., Eck, T. F., Breon, F.-M., Martonchik, J., Kahn, R., Diner, D. J., Vermote, E. F., Roger, J.-C., Lapyonok, T., and Slutsker, I.: Simultaneous retrieval of aerosol and surface properties from a combination of AERONET and satellite data, Remote Sens. Environ., 107, 90–108, doi:10.1016/j.rse.2006.07.022, 2007.

Smirnov, A., Holben, B. N., Eck, T. F., Dubovik, O., and Slutsker, I.: Clouds creening and quality control algorithms for the AERONET database, Remote Sens. Environ., 73, 337–349, 2000.

Smirnov, A., Holben, B. N., Kaufman, Y. J., Dubovik, O., Eck, T. F., Slutsker, I., Pietras, C., and Halthore, R. N.: Optical properties of atmospheric aerosol in maritime environments, J. Atmos. Sci., 59, 501–523, 2002.

Stamnes, K., Tsay, S., Wiscombe, W., and Jayaweera, K.: Numerically stable algorithm for discrete–ordinate-method radiative transfer in multiple scattering and emitting layered media, Appl. Optics, 27, 2502–2509, 1988.

Toledano, C., Cachorro, V. E., Berjon, A., de Frutos, A. M., Sorribas, M., de la Morena, B. A., and Goloub, P.: Aerosol optical depth and Ångström exponent climatology at El Arenosillo AERONET site (Huelva, Spain), Q. J. Roy. Meteor. Soc., 133, 795–807, doi:10.1002/qj.54, 2007.

Twomey, S.: Pollution and the planetary albedo, Atmos. Environ., 8, 1251–1256, doi:10.1016/0004-6981(74)90004-3, 1974.

Valenzuela, A., Olmo, F. J., Lyamani, H., Antón, M., Quirantes, A., and Alados-Arboledas, L.: Aerosol radiative forcing during African desert dust events (2005–2010) over Southeastern Spain, Atmos. Chem. Phys., 12, 10331–10351, doi:10.5194/acp-12-10331-2012, 2012a.

Valenzuela, A., Olmo, F. J., Lyamani, H., Antón, M., Quirantes, A., and Alados-Arboledas, L.: Classification of aerosol radiative properties during African desert dust intrusions over southeastern Spain by sector origins and cluster analysis, J. Geophys. Res., 117, D06214, doi:10.1029/2011JD016885, 2012b.

Valenzuela, A., Olmo, F. J., Lyamani, H., Granados-Muñoz, M. J., Antón, M., Guerrero-Rascado, J. L., Quirantes, A., Toledano, C., Pérez-Ramírez, D., and Alados-Arboledas, L.: Aerosol transport over the western Mediterranean basin: evidence of the contribution of fine

ACPD
doi:10.5194/acp-2015-823

particles to desert dust plumes over Alborán Island, J. Geophys. Res.-Atmos., 119, 14028–14044, doi:10.1002/2014JD022044, 2015.

ACPD

doi:10.5194/acp-2015-823

Table 1. Wavelengths of the AERONET sun-photometers at Ersa, Palma and Alborán and level 2.0 data availability during the period 2011–2014. In the last column the numbers below each month indicate the number of that month with data in the period 2011–2014.

Site	Wavelengths	2011	2012	2013	2014	2011–2014
Ersa	340, 380, 440, 500, 675, 870, 1020, 1640 nm	JFMAMJJASOND	J MJJASOND	JFMA	JFMAMJJASO	JFMAMJJASOND 433333333322
Palma	340, 380, 440, 500, 675, 870, 1020 nm	ASOND	MJJASOND	JFMAMJJASOND		JFMAMJJASOND 111122233333
Alborán	340, 380, 440, 500, 675, 870, 1020 nm	JJASOND	J			

ACPD
doi:10.5194/acp-2015-823

Table 2. Summary of the seasonal variations of the aerosol optical properties (AOD_{440}, $AE_{440-870}$, $AAOD_{440}$, $AAE_{440-870}$ and sphericity) at Ersa, Palma and Alborán. In the last column (E) and (I) indicate if the parameter is an extensive or intensive parameter, respectively.

		Summer (*N*) Mean ± SD	Autumn	Winter	Spring	Year	NE–SW gradient
AOD_{440}	Ersa	(13093) 0.18 ± 0.10	(6327) 0.13 ± 0.09	(2620) 0.09 ± 0.05	(6656) 0.16 ± 0.11	(28696) 0.16 ± 0.10	
	Palma	(8667) 0.23 ± 0.12	(6062) 0.16 ± 0.11	(1831) 0.07 ± 0.04	(2319) 0.10 ± 0.06	(18879) 0.18 ± 0.12	Yes (E)
	Alborán	(2233) 0.27 ± 0.14	(2167) 0.17 ± 0.11	(586) 0.08 ± 0.03	(0) –	(4986) 0.20 ± 0.13	
$AE_{440-870}$	Ersa	(13093) 1.44 ± 0.47	(6327) 1.46 ± 0.51	(2620) 1.14 ± 0.49	(6656) 1.28 ± 0.45	(28696) 1.38 ± 0.48	
	Palma	(8667) 1.14 ± 0.47	(6062) 1.21 ± 0.48	(1831) 1.11 ± 0.43	(2319) 0.99 ± 0.34	(18879) 1.14 ± 0.46	Yes (I)
	Alborán	(2233) 0.61 ± 0.33	(2167) 1.02 ± 0.36	(586) 0.85 ± 0.36	(0) –	(4986) 0.81 ± 0.40	
$AAOD_{440}$	Ersa	(26) 0.018 ± 0.011	(12) 0.023 ± 0.017	(0) –	(11) 0.035 ± 0.027	(49) 0.023 ± 0.018	
	Palma	(57) 0.043 ± 0.019	(25) 0.034 ± 0.021	(0) –	(0) –	(82) 0.040 ± 0.020	No (E)
	Alborán	(15) 0.016 ± 0.010	(0) –	(0) –	(0) –	(15) 0.016 ± 0.010	
$AAE_{440-870}$	Ersa	(26) 1.64 ± 0.52	(12) 1.28 ± 0.44	(0) –	(11) 2.11 ± 0.89	(49) 1.66 ± 0.66	
	Palma	(57) 1.98 ± 0.49	(25) 1.64 ± 0.55	(0) –	(0) –	(82) 1.88 ± 0.53	No (I)
	Alborán	(15) 1.05 ± 0.26	(0) –	(0) –	(0) –	(15) 1.05 ± 0.26	
Sphericity	Ersa	(321) 57 ± 45	(92) 87 ± 31	(8) 74 ± 46	(142) 75 ± 38	(563) 67 ± 43	
%	Palma	(408) 41 ± 41	(145) 69 ± 40	(0) –	(13) 60 ± 43	(566) 49 ± 42	Yes (I)
	Alborán	(85) 25 ± 32	(66) 38 ± 37	(0) –	(0) –	(151) 31 ± 35	

ACPD
doi:10.5194/acp-2015-823

Table 3. Summary of the seasonal variations of the aerosol microphysical properties (size distribution and refractive index) at Ersa, Palma and Alborán. r_V and C_V are the volume median radius and the volume concentration, respectively. f/c indicate fine and coarse modes, respectively. In the last column (E) and (I) indicate if the parameter is an extensive or intensive parameter, respectively.

		Summer (*N*) Mean ± SD	Autumn	Winter	Spring	Year	NE–SW gradient
r_V^f	Ersa	(993) 0.16 ± 0.02	(538) 0.17 ± 0.02	(158) 0.18 ± 0.03	(518) 0.17 ± 0.02	(2207) 0.17 ± 0.02	
µm	Palma	(809) 0.14 ± 0.02	(548) 0.15 ± 0.02	(177) 0.15 ± 0.02	(184) 0.15 ± 0.02	(1718) 0.15 ± 0.02	No (I)
	Alborán	(164) 0.17 ± 0.02	(175) 0.18 ± 0.02	(34) 0.19 ± 0.02	(0) –	(373) 0.18 ± 0.02	
C_V^f	Ersa	(993) 0.019 ± 0.012	(538) 0.014 ± 0.011	(158) 0.009 ± 0.006	(518) 0.019 ± 0.013	(2207) 0.017 ± 0.012	
$\mu m^3\,\mu m^{-2}$	Palma	(809) 0.025 ± 0.013	(548) 0.021 ± 0.017	(177) 0.010 ± 0.007	(184) 0.011 ± 0.008	(1718) 0.021 ± 0.014	No (E)
	Alborán	(164) 0.023 ± 0.011	(175) 0.021 ± 0.012	(34) 0.012 ± 0.005	(0) –	(373) 0.021 ± 0.011	
r_V^c	Ersa	(993) 2.49 ± 0.41	(538) 2.73 ± 0.43	(158) 2.73 ± 0.44	(518) 2.27 ± 0.46	(2207) 2.52 ± 0.46	
µm	Palma	(809) 2.43 ± 0.41	(548) 2.61 ± 0.37	(177) 2.43 ± 0.37	(184) 2.10 ± 0.44	(1718) 2.46 ± 0.42	Yes (I)
	Alborán	(164) 2.33 ± 0.45	(175) 2.53 ± 0.47	(34) 2.70 ± 0.38	(0) –	(373) 2.46 ± 0.47	
C_V^c	Ersa	(993) 0.032 ± 0.036	(538) 0.021 ± 0.040	(158) 0.018 ± 0.021	(518) 0.027 ± 0.053	(2207) 0.027 ± 0.041	
$\mu m^3\,\mu m^{-2}$	Palma	(809) 0.063 ± 0.063	(548) 0.038 ± 0.052	(177) 0.013 ± 0.011	(184) 0.025 ± 0.021	(1718) 0.046 ± 0.056	Yes (E)
	Alborán	(164) 0.083 ± 0.063	(175) 0.050 ± 0.041	(34) 0.019 ± 0.012	(0) –	(373) 0.062 ± 0.055	
RRI_{440}	Ersa	(26) 1.45 ± 0.03	(12) 1.46 ± 0.06	(0) –	(11) 1.44 ± 0.04	(49) 1.45 ± 0.04	
	Palma	(57) 1.43 ± 0.05	(25) 1.42 ± 0.06	(0) –	(0) –	(82) 1.43 ± 0.06	No (I)
	Alborán	(15) 1.44 ± 0.06	(0) –	(0) –	(0) –	(15) 1.44 ± 0.06	
IRI_{440} ($\times 10^3$)	Ersa	(26) 2.6 ± 1.3	(12) 3.6 ± 1.8	(0) –	(11) 3.6 ± 1.3	(49) 3.1 ± 1.3	
	Palma	(57) 4.7 ± 1.6	(25) 4.8 ± 2.3	(0) –	(0) –	(82) 4.7 ± 1.8	No (I)
	Alborán	(15) 1.5 ± 0.8	(0) –	(0) –	(0) –	(15) 1.5 ± 0.8	

ACPD
doi:10.5194/acp-2015-823

Table 4. Summary of the seasonal variations of the aerosol radiative properties (SSA_{440} and g_{440}) and the solar radiative forcing and forcing efficiency at Ersa, Palma and Alborán. In the last column (E) and (I) indicate if the parameter is an extensive or intensive parameter, respectively.

		Summer (N) Mean ± SD	Autumn	Winter	Spring	Year	NE–SW gradient
SSA_{440}	Ersa	(26) 0.96 ± 0.02	(12) 0.96 ± 0.02	(0) –	(11) 0.94 ± 0.02	(49) 0.96 ± 0.03	
	Palma	(57) 0.92 ± 0.03	(25) 0.93 ± 0.04	(0) –	(0) –	(82) 0.92 ± 0.03	No (I)
	Alborán	(15) 0.97 ± 0.02	(0) –	(0) –	(0) –	(15) 0.97 ± 0.02	
g_{440}	Ersa	(993) 0.69 ± 0.02	(538) 0.70 ± 0.03	(158) 0.72 ± 0.05	(518) 0.70 ± 0.03	(2207) 0.69 ± 0.03	
	Palma	(809) 0.69 ± 0.03	(548) 0.71 ± 0.03	(177) 0.68 ± 0.04	(184) 0.69 ± 0.03	(1718) 0.70 ± 0.03	No (I)
	Alborán	(164) 0.74 ± 0.02	(175) 0.75 ± 0.02	(34) 0.75 ± 0.02	(0) –	(373) 0.75 ± 0.02	
ARF_{BOA}	Ersa	(413) −17.5 ± 9.5	(205) −13.6 ± 10.0	(23) −17.6 ± 8.3	(195) −18.0 ± 9.2	(836) −16.7 ± 9.7	
$W\,m^{-2}$	Palma	(282) −22.8 ± 13.4	(193) −16.5 ± 12.1	(14) −6.7 ± 3.3	(65) −9.6 ± 6.0	(554) −18.7 ± 13.2	Yes (E)
	Alborán	(63) −27.8 ± 13.8	(75) −18.3 ± 10.4	(8) −14.8 ± 11.8	(0) –	(146) −22.2 ± 13.0	
ARF_{TOA}	Ersa	(413) −12.8 ± 7.0	(205) −9.7 ± 6.6	(23) −7.4 ± 4.9	(195) −10.9 ± 5.7	(836) −11.4 ± 6.7	
$W\,m^{-2}$	Palma	(282) −13.0 ± 6.8	(193) −10.7 ± 6.5	(14) 5.5 ± 2.8	(65) −6.9 ± 3.6	(554) −11.3 ± 6.7	No (E)
	Alborán	(63) −18.8 ± 10.4	(75) −13.4 ± 7.7	(8) −6.0 ± 1.8	(0) –	(146) −15.3 ± 9.5	
$ARFE_{BOA}$	Ersa	(413) −139.1 ± 23.6	(205) −137.8 ± 18.8	(23) −182.9 ± 31.4	(195) −157.9 ± 39.7	(836) −144.4 ± 29.3	
$W\,m^{-2}AOD_{550}^{-1}$	Palma	(282) −136.4 ± 40.9	(193) −129.6 ± 27.4	(14) −130.7 ± 13.9	(65) −122.0 ± 24.6	(554) −132.2 ± 34.8	No (I)
	Alborán	(63) −142.1 ± 30.4	(75) −132.5 ± 49.0	(8) −191.4 ± 85.5	(0) –	(146) −139.9 ± 46.4	
$ARFE_{TOA}$	Ersa	(413) −101.2 ± 10.2	(205) −100.7 ± 12.1	(23) −74.7 ± 11.6	(195) −96.3 ± 15.1	(836) −99.2 ± 12.8	
$W\,m^{-2}\,AOD_{550}^{-1}$	Palma	(282) −79.7 ± 18.9	(193) −88.5 ± 15.4	(14) −107.0 ± 13.3	(65) −93.8 ± 12.9	(554) −85.1 ± 18.1	No (I)
	Alborán	(63) −91.9 ± 7.3	(75) −95.5 ± 13.8	(8) −94.0 ± 30.0	(0) –	(146) −93.8 ± 12.9	

ACPD
doi:10.5194/acp-2015-823

Figure 1. Geographical situation of Ersa, Palma and Alborán in the WMB.

ACPD
doi:10.5194/acp-2015-823

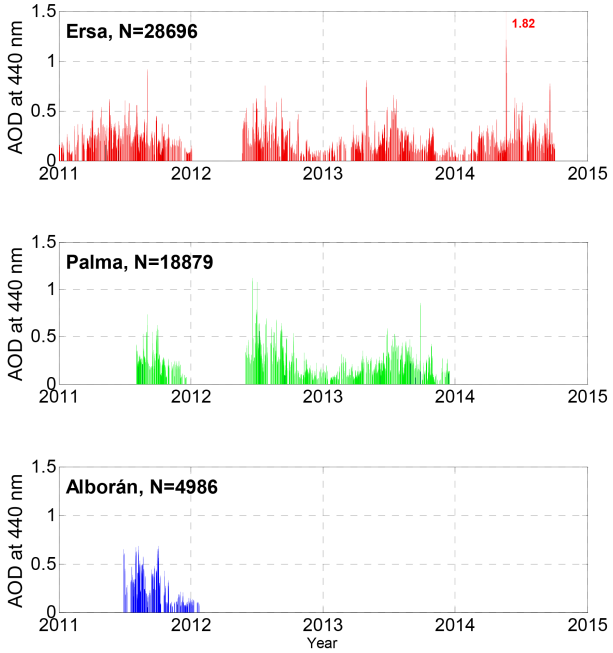

Figure 2. Instantaneous AOD at 440 nm at the three sites during the period 2011–2014. In this figure and in the rest of the paper *N* represents the number of points used in the plot shown.

ACPD
doi:10.5194/acp-2015-823

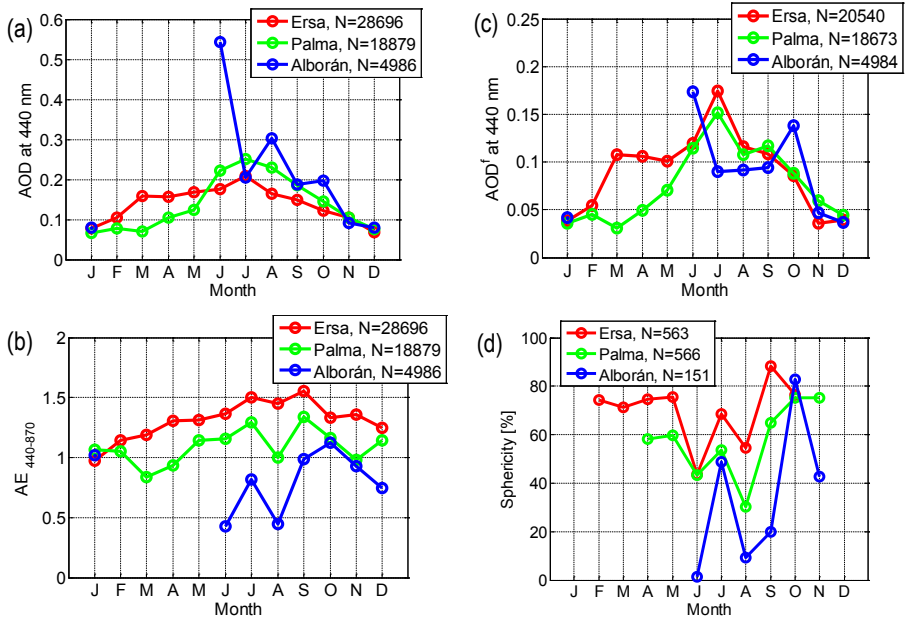

Figure 3. Monthly average variations over the whole dataset of **(a)** AOD_{440}; **(b)** $AE_{440-870}$; **(c)** AOD^{f}_{440} and **(d)** the sphericity.

ACPD
doi:10.5194/acp-2015-823

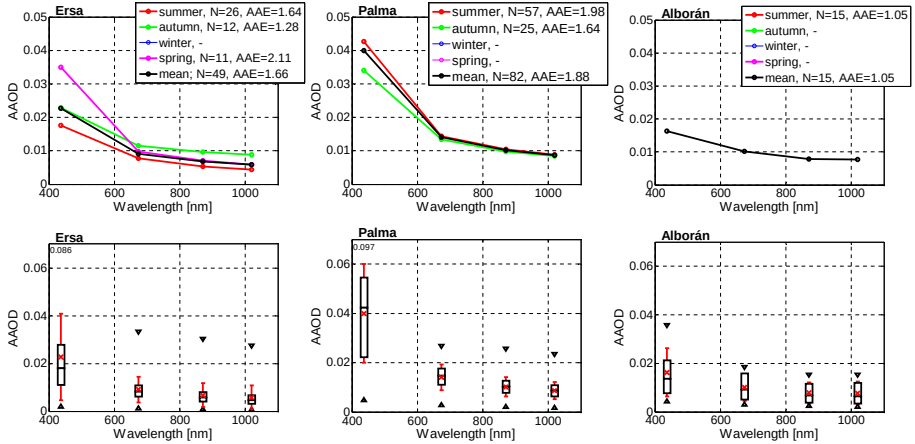

Figure 4. (top) Seasonal variation of the spectral AAOD at the three sites. (bottom) Box-and-whisker plots (median, first and third quartile and minimum and maximum values) representing the spectral AAOD on an annual basis at the three sites. The red whiskers represent the standard deviation around the mean value (red cross sign). Upward and downward triangles indicate minimum and maximum values, respectively.

ACPD
doi:10.5194/acp-2015-823

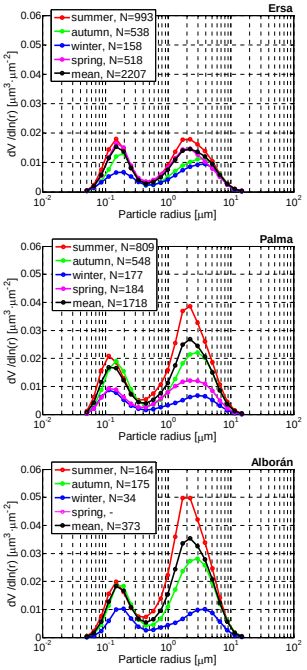

Figure 5. Seasonal variation of the volume size distribution at the three sites.

ACPD
doi:10.5194/acp-2015-823

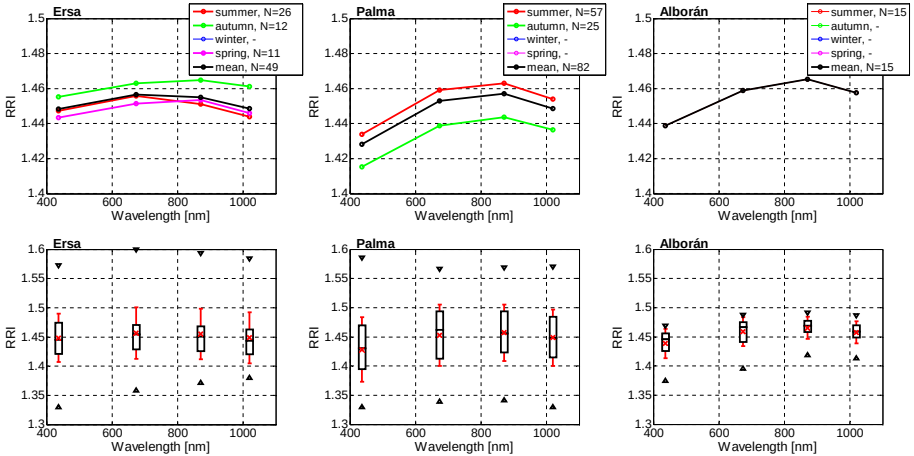

Figure 6. Same as Fig. 4 for the spectral real part of the refractive index (RRI) at the three sites.

ACPD
doi:10.5194/acp-2015-823

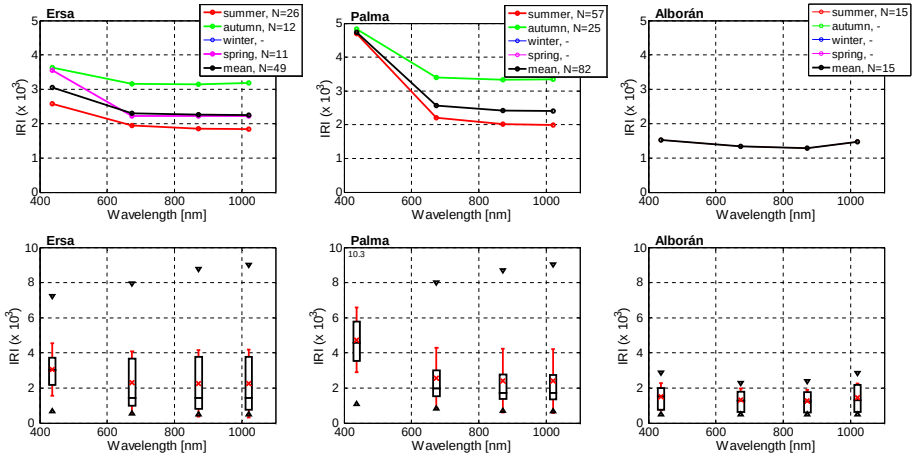

Figure 7. Same as Fig. 4 for the spectral imaginary part of the refractive index (IRI) at the three sites.

ACPD
doi:10.5194/acp-2015-823

Aerosol optical, microphysical and radiative properties

M. Sicard et al.

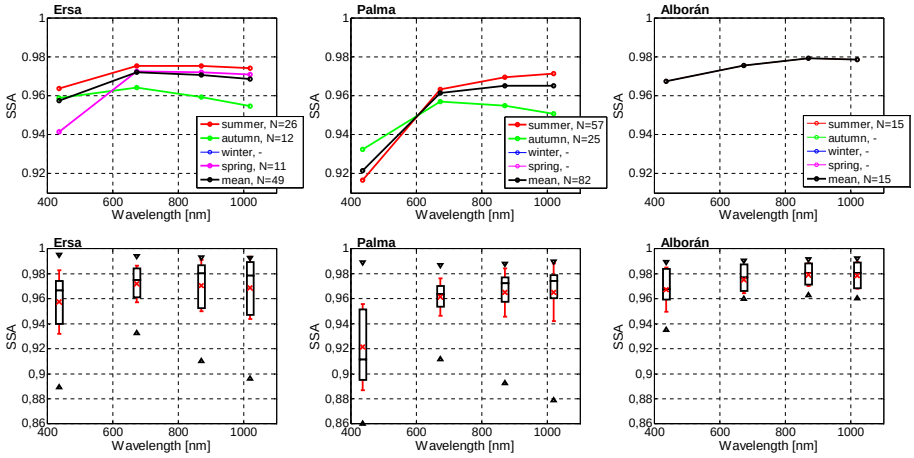

Figure 8. Same as Fig. 4 for the spectral SSA at the three sites.

ACPD
doi:10.5194/acp-2015-823

Aerosol optical, microphysical and radiative properties

M. Sicard et al.

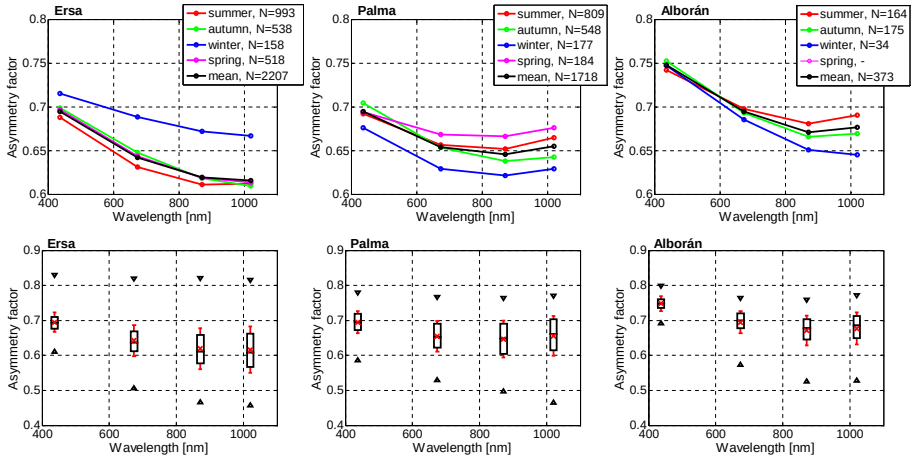

Figure 9. Same as Fig. 4 for the spectral asymmetry factor at the three sites.

ACPD
doi:10.5194/acp-2015-823

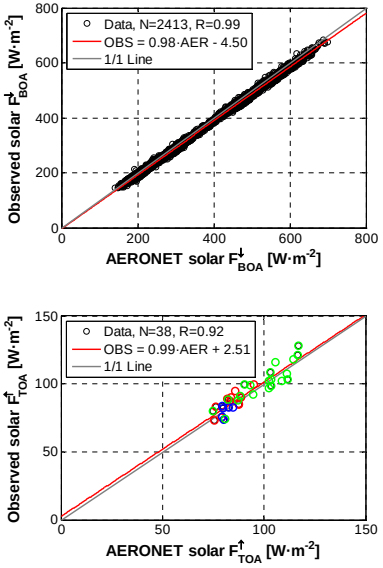

Figure 10. (a) Observed SolRad-Net level 1.5 vs. modeled AERONET level 2.0 solar downward fluxes at the surface in Barcelona over the period May 2009–October 2014. **(b)** Observed CERES vs. modeled AERONET level 1.5 solar upward fluxes at the TOA in Ersa (red circles), Palma (green circles) and Alborán (blue circles).

ACPD
doi:10.5194/acp-2015-823

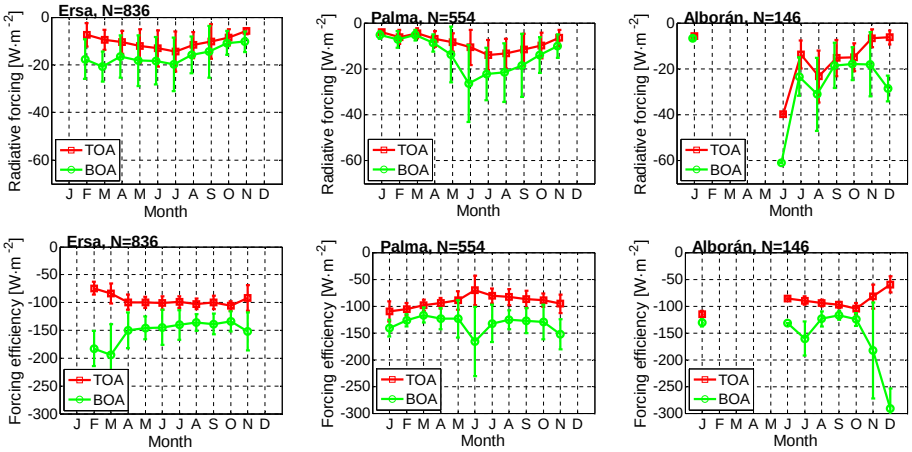

Figure 11. Seasonal variation of (top) the solar radiative forcing and of (bottom) the solar radiative forcing efficiency. Both the ARF and the ARFE were estimated for $50 \leq SZA \leq 60^{\circ}$.

ACPD
doi:10.5194/acp-2015-823

Aerosol optical, microphysical and radiative properties

M. Sicard et al.

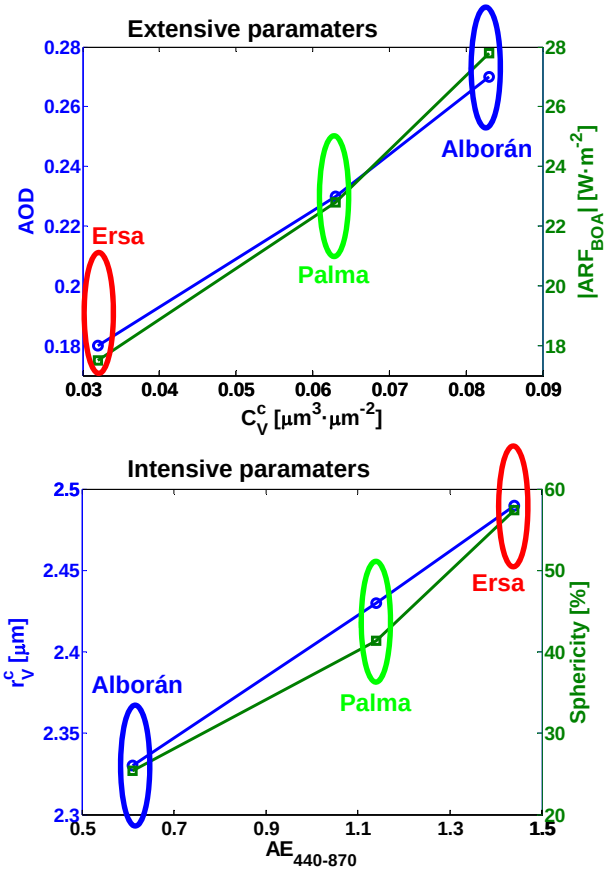

Figure 12. Summer NE–SW gradient for **(a)** extensive parameters (AOD_{440}, C_V^c and ARF_{BOA}) and for **(b)** intensive parameters ($AE_{440-870}$, r_V^c and the sphericity).

ACPD
doi:10.5194/acp-2015-823